Review of SPECT collimator selection, optimization, and fabrication for clinical and preclinical imaging

Karen Van Audenhaege,[a] Roel Van Holen, Stefaan Vandenberghe, and Christian Vanhove
Department of Electronics and Information Systems, MEDISIP-IBiTech, Ghent University–iMinds Medical IT, De Pintelaan 185 block B/5, Ghent B-9000, Belgium

Scott D. Metzler
Department of Radiology, University of Pennsylvania, Philadelphia, Pennsylvania 19104

Stephen C. Moore
Division of Nuclear Medicine, Department of Radiology, Brigham and Women's Hospital and Harvard Medical School, 75 Francis Street, Boston, Massachusetts 02115

(Received 31 March 2015; revised 7 July 2015; accepted for publication 8 July 2015; published 24 July 2015)

In single photon emission computed tomography, the choice of the collimator has a major impact on the sensitivity and resolution of the system. Traditional parallel-hole and fan-beam collimators used in clinical practice, for example, have a relatively poor sensitivity and subcentimeter spatial resolution, while in small-animal imaging, pinhole collimators are used to obtain submillimeter resolution and multiple pinholes are often combined to increase sensitivity. This paper reviews methods for production, sensitivity maximization, and task-based optimization of collimation for both clinical and preclinical imaging applications. New opportunities for improved collimation are now arising primarily because of (i) new collimator-production techniques and (ii) detectors with improved intrinsic spatial resolution that have recently become available. These new technologies are expected to impact the design of collimators in the future. The authors also discuss concepts like septal penetration, high-resolution applications, multiplexing, sampling completeness, and adaptive systems, and the authors conclude with an example of an optimization study for a parallel-hole, fan-beam, cone-beam, and multiple-pinhole collimator for different applications. [http://dx.doi.org/10.1118/1.4927061]

Key words: SPECT, collimator, production, single photon emission computed tomography, optimization

1. INTRODUCTION

Single photon emission computed tomography (SPECT) relies on the tracer principle[1] to image physiological functions. A tracer is injected intravenously into the bloodstream of the patient and participates in the body's metabolism and distributes accordingly. Following radioactive decay, photons will be emitted in all directions and exit the body to be detected by a gamma camera. In order to reconstruct the original location of the source, information about the incident angle of the detected photons on the detector is needed. Therefore, a collimator, which maps lines of response to particular detector positions, is used. In most clinical systems [e.g., Fig. 1(a)], the collimator is mounted on a flat detector head that rotates around the patient to acquire projection data at different angles. An iterative reconstruction algorithm or an analytic approach [e.g., filtered back projection (FBP)] can then be used to reconstruct the three-dimensional (3D) distribution of the radioactive tracer. In fact, the reconstructed SPECT image is actually a blurred version of the true activity distribution, due to the finite resolution of the system. Spatial resolution is an important system property and is expressed as the full-width-at-half-maximum (FWHM) of the point spread function (PSF), which is determined by the detector intrinsic resolution and the geometrical resolution of the collimator. Another important system property is sensitivity, i.e., the ratio of emitted versus detected photons. Both sensitivity and resolution can have different values across the field of view (FOV) but most manufacturers only mention one value. When comparing different systems, it is therefore important to understand which value is used. Sensitivity can be, e.g., a peak value, the value at the center of the FOV or an average over the complete FOV (volume sensitivity). It can be calculated theoretically or measured experimentally (in which case it might include attenuation in the phantom). Spatial resolution is often calculated in the center of the FOV or measured by evaluating the smallest rods that can be distinguished in a cold/hot rod phantom.

Despite the growth of positron emission tomographic (PET) examinations in recent years, the number of SPECT procedures has remained stable or even increased, e.g., in Europe.[2] SPECT radionuclides have an intermediate half-life—typically ranging from a few hours to a few days—and can, therefore, be produced in large quantities and distributed by pharmaceutical companies. PET tracers, on the other hand, have a half-life ranging from a few seconds to a few hours, so that more remote hospitals need to have their own cyclotron infrastructure, which drastically increases the

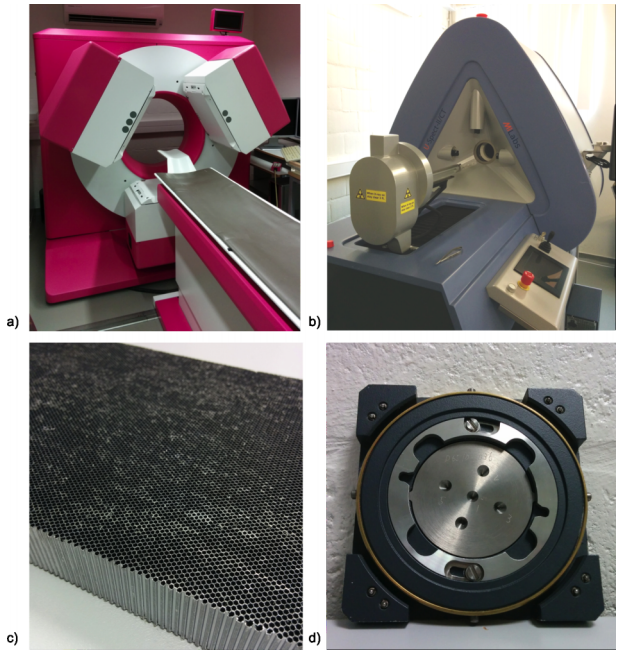

FIG. 1. (a) The Prism 3000XP from Picker (Philips): a clinical triple-head SPECT system (b) The U-SPECT II from MILabs: A preclinical stationary SPECT system (c) A parallel-hole collimator (d) A multiple-pinhole collimator.

operational costs. The most commonly used radionuclide for SPECT is 99m-technetium (^{99m}Tc), which has a main photo peak at 140.5 keV and a half-life of 6.01 h. ^{99m}Tc-labeled hexamethyl propyleneamine oxime (HMPAO) is one example of a SPECT tracer that is widely used in clinical practice for inflammation and for cerebral perfusion imaging.[3] It is also used for ictal SPECT in focal epilepsy, as an alternative to ^{99m}Tc-labeled ethyl cysteinate dimer (ECD). Other ^{99m}Tc-based tracers are ^{99m}Tc-sestamibi, with applications in cardiac imaging[4] and oncology, ^{99m}Tc-methylene diphosphonate (MDP) for bone scintigraphy,[5] and ^{99m}Tc-labeled colloids for sentinel lymph node visualization. Other radionuclides include, for example, ^{111}In and ^{123}I with ^{111}In being used in octreotide scans for diagnosing carcinoid tumors[3] and paragangliomas[6] and with the latter being most commonly used as Na^{123}I for the evaluation of thyroid disease[7] and in, e.g., ^{123}I-*N*-omega-fluoropropyl-2beta-carbomethoxy-3beta-(4-iodophenyl)nortropan (FP-CIT)[8] and ^{123}I-iodobenzamide (IBZM)[9] for the diagnosis of Parkinson's and Huntington's diseases. The same radiotracers are also used in small animals for preclinical and translational studies.[10] For the development of new tracers and new therapies, (small) animal studies are performed using representative animal models.

Every application has its own specific requirements for sensitivity and resolution. For example, in small animals, resolution is generally more important than in most human whole-body clinical applications. In gated cardiac imaging, on the other hand, sensitivity is generally considered to be more important than resolution. Furthermore, imaging of higher energy radionuclides presents additional challenges for reducing collimator penetration and scatter without seriously compromising either resolution or sensitivity. Differences in system requirements have been primarily responsible for the development of both new imaging systems and collimators.

Collimators are made of materials with a high density and a high atomic number, such as lead, tungsten, gold, and platinum; they have holes that allow only those photons traveling along desired paths to pass through. Only a small fraction (typically $\sim 10^{-4}$–10^{-2}) of emitted photons pass through the holes and are detected, which seriously limits sensitivity. Making the holes bigger increases the sensitivity but degrades the resolution; this effect is often called the resolution-sensitivity trade-off and it depends on a complicated manner on many parameters, such as the size of the region of interest (ROI) or organ(s) being imaged, the type of collimator (pinhole, parallel-hole, fan-beam, etc.), the energy of the photon(s) to be detected, the detector's intrinsic spatial resolution, the size of the detector, and the radius of rotation (ROR).

The principles of collimator design were extensively described in a review article in 1992 (Ref. 11) and in several textbook chapters; e.g., see the work of Gunter[12] and Meikle *et al.*[13] for clinical and preclinical collimators, respectively. More recently there have been many new developments in collimator-production techniques, which make the fabrication of more complex collimator designs possible.

New detector technologies, providing better intrinsic spatial resolution, have also become available. For example, detectors based on (digital) silicon photomultipliers (SiPM) coupled to a thin monolithic crystal were shown to have an intrinsic spatial resolution of 0.5–2 mm.[14–16] Direct conversion detectors, like cadmium zinc telluride (CZT) detectors, have an intrinsic resolution that is largely determined by the pixel pitch and can be submillimeter.[17] A detailed discussion of SPECT detectors is outside the scope of this paper but the interested reader is referred to the work of Peterson and Furenlid.[18] Nevertheless, the recent improvements in detector resolution have influenced the optimal collimator requirements. High-resolution (HR) detector technologies call for a collimator with smaller magnification[19–21] and allow more projections on the detector, which is beneficial for stationary SPECT systems. These offer potential advantages for dynamic scanning, for improved system stability and patient comfort, and for compatibility with MRI, enabling the development of truly simultaneous SPECT/MR for both preclinical and clinical use.[22–25]

Finally, there are several new insights on the use of multiplexed data from multiple-pinhole SPECT systems,[26–29] as well as on combining hybrid data from different types of collimation[29–34] that will be discussed in Sec. 1.E.

The purpose of this review is to provide some insights and useful guidelines for choosing, optimizing, and producing SPECT collimators with the latest developments in mind. In the Introduction, we first give an overview of the different collimator types with their characteristics (sensitivity and resolution). We then discuss some key concepts like septal penetration, high-energy applications, sampling completeness, and multiplexing. We also discuss different manufacturing techniques and their respective advantages and disadvantages. In the second part of this paper, we give some

general guidelines for selecting the best collimator type for different applications and target resolutions and in the last part, we introduce methods for sensitivity maximization and task-based collimator optimization. Finally, to conclude, we also give an example and use the optimization methods to compare a parallel-hole, fan-beam, cone-beam, and multiple-pinhole collimator for a few different applications.

1.A. Collimator types

The decision about which type of collimator to use for a given imaging application depends most importantly on the ratio between the size of the FOV, the size of the imaging detector and the required spatial resolution and/or sensitivity. Therefore, we shall first review several different types of collimation with their specific sensitivity and resolution properties. For simplicity, the collimator resolution formulae shown in this section do not include the mean interaction depth in the detector, which is generally much smaller than the distance from the source to the collimator and the collimator thickness.

1.A.1. Parallel-hole collimators

The parallel-hole collimator was first presented by Anger in 1964 (Ref. 35) and is still used as the standard collimator in clinical practice. The collimator consists of a plate of dense material (most commonly an alloy of lead and a few percent antimony) containing a honeycomb structure of closely packed, parallel, hexagonal-shaped holes separated by lead septa [Fig. 1(c)]. Other hole shapes (e.g., square, circular, or triangular) also exist, but are less common. Figure 2(a) shows a cross section. Only photons traveling within a tight cone-shaped region in a direction perpendicular to the entrance surface of the collimator have a chance of fully traversing a collimator hole. Only those photons that are not absorbed by the collimator material can reach the detector. A parallel-hole collimator with hexagonal holes and a perfectly absorbing detector has a point-source sensitivity of[35–37]

$$\mathrm{Sens}_{\mathrm{paho}} = \frac{\sqrt{3}}{8\pi}\frac{d^2}{a_{\mathrm{eff}}^2}\frac{d^2}{(d+t)^2} \tag{1}$$

and a resolution of[35,38,39]

$$R_{\mathrm{paho}}(h) = d\frac{a+h}{a_{\mathrm{eff}}}, \tag{2}$$

respectively, where d is the hole diameter (flat-to-flat distance), t is the septal thickness, and h is the perpendicular distance from the point source to the detector. $a_{\mathrm{eff}} = a - 2/\mu$ is the physical hole length a (collimator thickness) approximately adjusted for penetration effects.[38] μ is the attenuation coefficient ($1/\mu = 0.37$ mm for $^{99\mathrm{m}}$Tc and lead). The system resolution is

$$R_{\mathrm{sys}}(h) = \sqrt{R_i^2 + [R_{\mathrm{paho}}(h)]^2}, \tag{3}$$

where R_i is the intrinsic spatial resolution of the detector. Both sensitivity and resolution formulae are given for a point source at a certain location in image space. For a parallel-hole system, the point source sensitivity is equal everywhere in the FOV, while resolution depends on the distance h. For the analytical derivation of the formulae and for other hole shapes, the reader is referred to the work of Wieczorek and Goedicke.[37]

1.A.2. Converging and diverging hole collimators

When the object of interest is smaller than the available detector area, an important performance gain may result from using converging collimators; this is because, for a small object, a parallel-hole collimator would leave most of the detector unused. For this reason, clinical brain SPECT imaging is often performed using fan-beam and not parallel-hole collimators. In a fan-beam collimator, the holes converge toward a focal line parallel to the axis of rotation [Fig. 2(b)]. The holes are tilted in the transverse plane and parallel in the axial direction. In a cone-beam collimator, the holes are tilted both in the transverse plane and in the axial direction, and converge toward a focal point. Converging collimators magnify the ROI on the detector and, therefore, the intrinsic resolution of the detector, R_i, is improved to $R_i/(m_{\mathrm{conv}}(h))$ in the object,

$$R_{\mathrm{sys}}(h,\theta) = \sqrt{\left(\frac{R_i}{m_{\mathrm{conv}}(h)}\right)^2 + [R_{\mathrm{conv}}(h,\theta)]^2}, \tag{4}$$

where $m_{\mathrm{conv}}(h)$ is the collimator magnification, defined as

$$m_{\mathrm{conv}}(h) = \frac{f+a}{f-h} \tag{5}$$

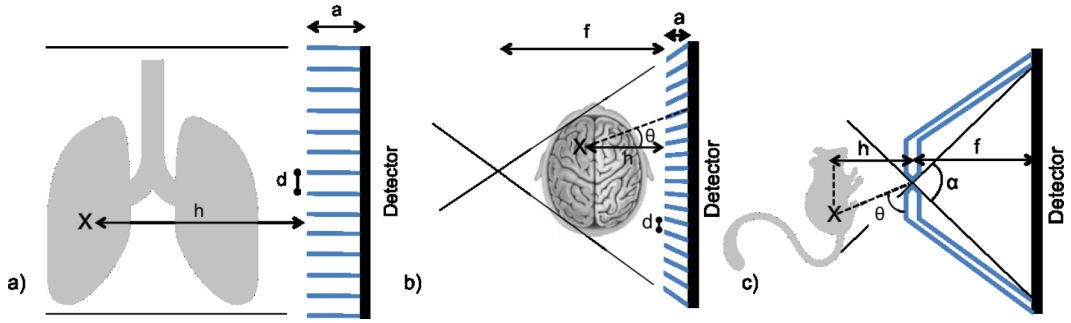

FIG. 2. Transverse cut through a (a) parallel-hole collimator (b) fan beam collimator (c) pinhole collimator.

and f is the focal length and $R_{\text{conv}}(h,\theta)$ is the geometric resolution of the collimator,

$$R_{\text{conv}}(h,\theta) = d\frac{a+h}{a_{\text{eff}}}\frac{1}{\cos\theta}\frac{f+a/2}{f+a}, \tag{6}$$

where θ is the angle between the detected gamma ray and the perpendicular to the detector ($\theta = 0$ for perpendicular incidence).

This resolution formula is based on the derivation given by Moyer[40] and the letter from Gerber[39] addressing the effect of collimator penetration.

The sensitivity of the converging hole collimator is

$$\text{Sens}_{\text{conv}}(h,\theta) = \frac{\sqrt{3}}{8\pi}\frac{d^2}{a_{\text{eff}}^2}\frac{d^2}{(d+t)^2}\left(\frac{f}{f-h}\right)^n \cos^2\theta, \tag{7}$$

where $n = 1$ for fan-beam collimators and $n = 2$ for cone-beam collimators.

The above resolution and sensitivity formulae are for a point source at a certain position in image space (where the position is determined by distance h and angle θ) and assume that the hole size is constant over the full length of the hole, and that it is identical for all holes.[11,40] Different formulae apply to different hole shapes,[37,41] and it has also been shown that hole tapering provides improved sensitivity at equal resolution.[42,43]

When the object of interest is relatively large, it may be appropriate to use diverging collimators,[44] e.g., for kinetic modeling in mice, it is important to see the organ of interest and the heart within a single bed position in order to obtain an arterial input curve.[45] Although diverging collimators have not been very common in the past, with the arrival of new high-resolution detector technologies, it becomes possible to enlarge the FOV and still obtain a sufficiently high resolution.[46]

1.A.3. (Multiple-)pinhole collimators

A pinhole collimator consists of a small pinhole aperture in a plate of lead, tungsten, or any other dense material [Figs. 2(c) and 1(d)]. The object of interest is projected through the aperture onto the detector. The most common pinhole has a knife-edge profile [Fig. 2(c)] but other shapes, e.g., channeled (keel-edge) pinholes, have also been used.[47] Keel-edge pinholes are particularly interesting for high-energy radionuclides and pinholes with large acceptance angles, as they reduce penetration. Other solutions to reduce penetration include the use of truncated pinholes[48] or clustered pinholes.[49]

The resolution and sensitivity of a knife-edge pinhole collimator for a point source are[50]

$$\text{Sens}_{\text{piho}}(h,\theta) = \frac{d_{\text{Seff}}^2 \sin^3\theta}{16h^2}, \tag{8}$$

where θ and h determine the location of the point source in image space, with θ the angle of incidence measured from the plane of the pinhole aperture ($\theta = \pi/2$ for perpendicular incidence) and h the perpendicular distance from the point in the FOV to the plane defined by the pinhole aperture. d_{Seff} is the sensitivity-effective pinhole diameter, which is the physical pinhole diameter, d, corrected for penetration at the edges of the aperture at normal incidence,[50,51]

$$d_{\text{Seff}} = \sqrt{d\left(d + \frac{2}{\mu}\tan\frac{\alpha}{2}\right) + \frac{2}{\mu^2}\tan^2\frac{\alpha}{2}}, \tag{9}$$

where α is the opening angle of the pinhole and the attenuation coefficient μ for tungsten at 140.5 keV is 3.6 mm^{-1}.

$$R_{\text{piho}}(h,\theta) = \sqrt{\frac{R_i^2}{[m_{\text{piho}}(h)]^2} + \left(d_{\text{Reff}}(h,\theta)\left(1 + \frac{1}{m_{\text{piho}}(h)}\right)\right)^2}, \tag{10}$$

where $d_{\text{Reff}}(h,\theta)$ is the resolution-effective pinhole diameter (corrected for penetration) and $m_{\text{piho}}(h)$ is the pinhole magnification,

$$m_{\text{piho}}(h) = \frac{f}{h}, \tag{11}$$

where f is the focal length (the pinhole-to-detector distance).

When $\theta \neq \pi/2$, the resolution-effective diameter $d_{\text{Reff}}(h,\theta)$ is broken into a parallel and perpendicular component, which are described by two equations as follows:[52]

$$d_{\text{re}\parallel}(h,\theta) = d + \frac{\ln 2}{\mu}\left(\tan^2\frac{\alpha}{2} - \cot^2\theta\right)\cot\frac{\alpha}{2}\sin\theta, \tag{12}$$

$$d_{\text{re}\perp}(h,\theta) = \sqrt{\left(d + \frac{\ln 2}{\mu}\tan\frac{\alpha}{2}\sin\theta\right)^2 - \left(\frac{\ln 2}{\mu}\right)^2\cos^2\theta}, \tag{13}$$

where $d_{\text{re}\parallel}(h,\theta)$ and $d_{\text{re}\perp}(h,\theta)$ are the resolution-effective aperture sizes in the parallel and perpendicular directions, respectively. The parallel direction is the perpendicular projection of the vector from the center of the pinhole aperture to the point source, on the plane of the pinhole. The perpendicular direction is perpendicular to the parallel direction in the detector plane. One can thus choose to calculate pinhole resolution [Eq. (10)] in the two directions, or to pick the worst/best case at each position or to assume normal incidence, which results in an effective pinhole diameter d_{Reff},

$$d_{\text{Reff}} = d + \frac{\ln 2}{\mu}\left(\tan\frac{\alpha}{2}\right). \tag{14}$$

Pinhole collimators are often used in small-animal imaging because they allow for high magnification so that submillimeter resolution can be achieved. The sensitivity of a single pinhole collimator is rather low, but if the detector is large enough, it can be improved by combining multiple pinholes into a multiple-pinhole collimator. Examples of commercial small-animal multiple-pinhole SPECT systems are the U-SPECT,[53] the FastSPECT,[54] the NanoSPECT (Ref. 55), and the X-SPECT.[56] Multiple-pinhole collimators have also been used for other applications, like cardiac[57–59] and brain SPECT imaging.[20,60]

With the arrival of high-resolution detector technologies, different studies have also shown the potential of combining multiple-pinhole collimators and object-minifying pinhole-detector geometries.[19–21,61,62] Minifying multiple-pinhole collimators allows more projections on the detector, which is beneficial for stationary SPECT systems. Another possibility for obtaining more projections on the detector is to allow overlap between the projections of multiple pinholes (Fig. 5),

which is also referred to as multiplexing. On the other hand, multiplexed projection data contain less information (because it is impossible to determine the pinhole through which a photon traveled before it was detected) and this can result in artifacts in the reconstructed image. This will be discussed in more detail in Sec. 1.E.

1.A.4. Other types of collimation

1.A.4.a. Coded apertures. A coded-aperture mask is a specific arrangement of many pinholes (often >100) that has been applied in astronomy and in medical imaging [Fig. 3(a)]. A coded-aperture collimator can be regarded as a highly multiplexed pinhole collimator, and it allows substantially improved system sensitivity while maintaining very good spatial resolution. However, it has been shown that the increased sensitivity of coded apertures only provides an equivalent increase in image signal-to-noise ratio (SNR) for point sources or sparse distributions of point sources.[63] Coded apertures are, in a sense, just extremely multiplexed multiple-pinhole collimators and, as a result, they suffer from a similar trade-off between sensitivity and data ambiguity (Sec. 1.E). Coded apertures are most interesting for sparse activity distributions, and less so for nonsparse objects.[63,64] Nevertheless, they have been successfully applied to high-resolution small-animal imaging in some applications.[65–67]

1.A.4.b. (Multiple-slit) slit-slat. A slit-slat collimator can be regarded as a mixture of a pinhole and a parallel-hole collimator [Fig. 3(b)]. Most commonly, the slits are oriented parallel to the axis of rotation. They form long knife-edges so that the collimator has the properties of a pinhole collimator in the transverse plane.[67] Between the knife-edges and the detector, parallel slats collimate the radiation in the axial direction. Slit-slat collimators combine the advantages of both the pinhole and the parallel-hole collimator: the pinholes magnify the ROI so that a high spatial resolution can be achieved (in the transverse plane). They are well suited for fully stationary systems as multiple slits can be combined in a ring around the FOV (multiple-slit slit-slat) providing sufficient angular sampling, while the parallel slats provide sufficient axial sampling. They are well-suited for medium-size objects with a long axial field of view, e.g., the human brain.[68]

1.A.4.c. Rotating slat. Rotating slat collimators are made of parallel slats, and thus collimate in only one direction. They measure plane integrals instead of line integrals. Therefore, SPECT data acquisition with slat collimators requires two motions: one rotation around the axial direction (similar to all other collimators) and one rotation around its own central axis.[69] Its system characteristics have been described in Ref. 70. Because the collimation is in only one direction, the sensitivity is much higher than that of a parallel-hole collimator. However, due to the large ambiguity, this increase in sensitivity does not necessarily result in better image quality, like in highly multiplexed multiple-pinhole systems. In planar scans with clinical phantoms, a rotating slat collimator performed better than a parallel-hole collimator,[71] but these results were not confirmed in the clinical setting of 3D-reconstructed heart-defect imaging.[72] Rotating slat collimators are well suited for "hot-spot" imaging (sparse objects), but are outperformed by parallel-hole collimators for imaging "cold" regions within a large background region (nonsparse objects).[73]

1.A.4.d. Hybrid collimators. Hybrid collimators combine different types of collimation. Examples are multisegment slant-hole,[74–76] variable angle slant-hole,[77,78] multifocal cone-beam,[79] and cardiofocal collimators,[80] as well as a hybrid ultra-short-cone-beam/slant-hole collimator.[81–83] They will not be further discussed here.

1.B. Septal penetration

Gamma rays that penetrate the collimator material can result in image degradation and need to be limited. In parallel-hole, fan-beam, and cone-beam collimators, penetration typically occurs when gamma rays cross from one collimator hole to the next. With thicker septa, there is less penetration; however, more of the detector area is obstructed, which degrades sensitivity. A proper trade-off is thus needed. A method for calculating the septal thickness, given a single-septal penetration of, e.g., 5% (which may be considered acceptable for some tasks), was described in Refs. 84 and 85. An even better solution is to include septal penetration in the optimization of the collimator.[86] For pinhole collimation, penetration typically occurs at the knife-edge of the pinholes, where the collimator material is thin. The degree of penetration is often very high but can be compensated during the reconstruction process by modeling the penetration during the ray-tracing process,[87] by using a mathematical description of the penetrative point-spread function,[88] or by

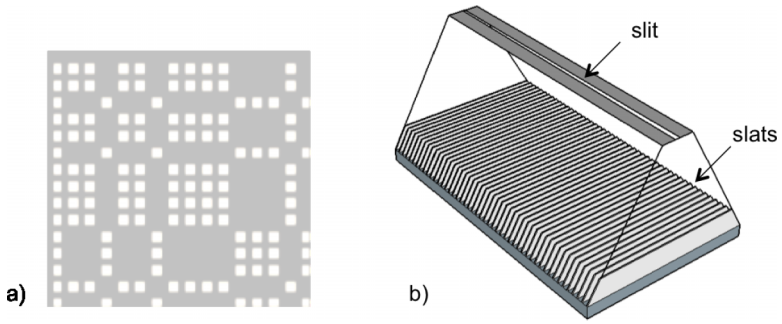

FIG. 3. (a) Coded-aperture collimator (b) slit-slat collimator.

using an effective pinhole aperture [Eqs. (9), (12), and (13)]. The degree of penetration is mainly influenced by the opening angle of the pinhole and the collimator material. Solutions for limiting septal penetration include the use of asymmetric pinholes,[48] pinholes with channels,[47,89] loftholes,[90] clustered pinholes,[49] and very high-density materials, such as gold or uranium. However, these are mostly needed to obtain very high resolution (submillimeter) with higher energy radionuclides, such as ^{18}F or ^{131}I, when the desired system resolution cannot be achieved anymore because of the high degree of penetration.[91]

1.C. High-energy applications

High-energy applications include imaging to follow patient response to therapy or to determine doses for radionuclide therapy, real-time proton beam range verification, and high-resolution tomography of positron emitters. These applications call for adapted collimator design because of the higher energy photons (above 300 keV up to MeV range) penetrating the collimator.

^{131}I is a beta-emitter and is frequently used for radionuclide therapy in lymphoma. Interestingly, it also emits gamma rays (mainly at 284, 364, 637, and 723 keV), which makes it possible to monitor the delivered dose. Van Holen *et al.*[92] showed improved quantification using a rotating slat collimator for ^{131}I compared to a parallel-hole collimator, due to a relative lower number of photons that penetrated the collimator.

Yttrium-90 is another radionuclide used frequently for cancer therapy by beta-emission (2.28 MeV). No gamma rays are emitted by this radionuclide; however, the betas generate secondary bremsstrahlung x-rays in the patient body that form a continuous spectrum extending up to the maximum electron energy. Walrand *et al.*[93] showed improved quantification using a camera with 30-mm thick BGO crystal and a high-energy pinhole collimator compared to a conventional NaI camera equipped with a high-energy parallel-hole collimator.

Hadron (proton and heavy ion) beam therapy is a radiotherapy treatment that is gaining importance, mainly because the hadron beams deliver their maximum energy within a defined range and heavy ions have a higher efficiency. Uncertainties in the determination of this range can be reduced using *in vivo* range verification. Therefore, Perali *et al.*[94] designed a tungsten slit collimator and used it to acquire prompt gamma rays in the 3–6 MeV energy range. Proton range verification is performed at projection level and is therefore not tomographic but nevertheless, we included it in this overview as an interesting high-energy application for slit collimators.

Finally, Goorden and Beekman[49] introduced the concept of clustered pinholes for the application of high-resolution tomography of ^{18}F, a positron emitter (511 keV). To deal with collimator edge penetration, every pinhole is replaced by a cluster of pinholes and every pinhole in a cluster has a narrow opening angle, which reduces photon penetration.

1.D. Sampling completeness

One of the major concerns when designing a collimator is the sampling completeness of the system. In the end, the purpose is to recover the 3D activity distribution from the projection data and this can only be successful if the acquired data contain sufficient information. We distinguish three types of sampling criteria: angular sampling, axial sampling, and the number of angular views.

1.D.1. Angular sampling

Conditions for angular sampling completeness in a parallel-hole system were first described by Orlov[95] and are, therefore, also called the Orlov conditions. Orlov showed that a single-head parallel-hole system needs to be continuously rotated over at least 180° to provide sufficient angular sampling (assuming no truncation in the FOV). Later, the sampling conditions were also evaluated for fan- and cone-beam collimators,[96,97] which need to be rotated over 180° plus the fan angle for sampling completeness, or over 360° in the case of a half-cone beam.[98] Pinholes and slits (at least those that see the complete transverse FOV) have a sampling profile similar to that of cone-beam collimators and require the same rotation. As an alternative, multiple pinholes or multiple slits can also be combined in a ring[25,53,60] or sphere[20,99] so that the system can be used without rotation.

1.D.2. Axial sampling

Tuy showed that cone-beam and pinhole systems only achieve data completeness in the plane described by the rotating focal point (mostly the central slice).[96] To obtain sufficient axial sampling in a longer object, they can be combined with a parallel-hole[100,101] or a fan-beam collimator[102–104] using a dual-head system. Alternatively, axial sampling sufficiency can also be obtained by scanning along a helical path.[105,106] However, one must be careful to use a sufficiently small helical pitch.[107] This helical movement can either be continuous or stepped, while acquiring data at each stop position of the camera, i.e., "step-and-shoot" mode. While helical orbits can also be used for pinhole collimators,[108,109] it is more common to use a multiple-pinhole collimator with pinholes focusing at different axial planes to improve sampling,[110,111] or to translate a cylindrical system with one or more ring(s) of pinholes.[53,112] One can even make a complete stationary system using multiple rings of pinholes focusing at different slices in the FOV (Ref. 60) or in a hemispherical configuration.[20,99]

In more complicated collimators (e.g., when the pinholes are tilted or truncated[48]), one can use a numerical algorithm to assess sampling completeness.[113] It is also common to evaluate axial sampling completeness using a reconstructed Defrise phantom,[114] a cylindrical phantom with a set of disks filled with activity [Fig. 4(a)]. It is advisable to use a phantom of the same size as the required FOV and to choose a disk thickness in the same range as the target resolution of the system.

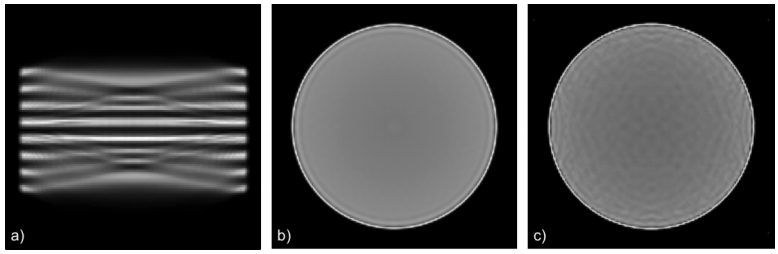

FIG. 4. (a) Insufficient axial sampling in a Defrise phantom (coronal view) (b) Sufficient angular sampling in a uniform phantom (transverse view) (c) Artifacts due to insufficient angular sampling in a uniform phantom (transverse view).

1.D.3. Angular views

The minimal number of angular views needed to reconstruct an object depends on the size of the object and the target resolution. In clinical whole-body and brain imaging, most systems rotate with a step size of 2°–6°. A stationary multiple-pinhole system for brain imaging would thus require 60–180 pinholes per axial slice. However, depending on the FOV and the magnification, the use of such a large number of pinholes might result in overlapping projections, which is usually undesired.

According to the Nyquist–Shannon sampling theorem,[115] the sampling period needs to be at least two times smaller than the target spatial resolution R_t. Therefore, we need a minimal number of projection angles per voxel of[116]

$$N_{\min} = \frac{\pi D}{R_t/2} \tag{15}$$

over a rotation angle of 360°, where D is the diameter of the FOV. For parallel-hole collimators, this also corresponds to the minimal number of rotation angles needed, while for pinholes, fan-beam collimator, and cone-beam collimator, a rebinning step is needed. However, other researchers have shown that the sampling requirement may be relaxed, at least for some types of projection geometries.[117,118] The optimal number of angular views also depends on the activity distribution,[119] the task, and the availability of prior information. A practical way to check the sampling period is to simulate or acquire a scan of a uniform phantom. Poor sampling will manifest itself through the presence of nonuniformity artifacts in the reconstructed image [Fig. 4(c)].

Providing sufficient angular views in a nonrotating system is very challenging. As an alternative to rotation, some multiple-pinhole systems include an axial/transverse translation to achieve sufficient sampling. For example, the U-SPECT (Ref. 53) achieves sufficient sampling in only a small region and uses small XYZ translations for imaging larger FOVs.[109] The T-SPECT achieves sufficient sampling using multiple-pinhole collimators mounted on two orthogonally positioned detectors[112] and a 3D-translation stage at 57 different locations. Sufficient angular sampling can also be obtained by translating the bed through a stationary multiple-pinhole system with pinholes positioned along a helix.

1.D.4. Sampling uniformity

We have now discussed axial and angular sampling sufficiency, but another important aspect of collimator design is sampling uniformity. When certain voxels in the FOV are sampled more often (and thus with a much higher sensitivity than others), this will result in different noise characteristics that will be visible when reconstructing a uniform phantom. This is often the case when using truncating pinholes. Another issue with truncating pinholes is that the peripheral regions of the pinhole's response are difficult to model. This results in streak artifacts and is particularly disturbing when this peripheral region is back-projected somewhere in the center of the FOV, as is the case with truncating pinholes. Luckily, these artifacts can be largely removed using rolled-off projection masks.[120]

1.E. Multiplexing

Figure 5 shows a multiple-pinhole system with overlapping pinholes. Most multiple-pinhole or multiple-slit slit-slat collimators are designed to allow no overlap between the different projections because the ambiguity introduced by multiplexing pinholes can result in artifacts. Some use baffles[121] or extra shielding[53] to remove overlap. Yet, there are examples of multiple-pinhole collimators that allow multiplexing and do not show any artifacts (e.g., Refs. 56 and 122) or only in certain phantoms.[123] Multiplexing also yields increased count sensitivity, since more pinholes can be placed on the collimator for the same detector size.

Over the last 10 yr, many interesting studies have provided useful insights about how to obtain artifact-free images with multiplexing systems, and whether or not the increased sensitivity also results in better image quality. For example, in at least three different systems, it has been observed that irregular pinhole patterns are less likely to produce

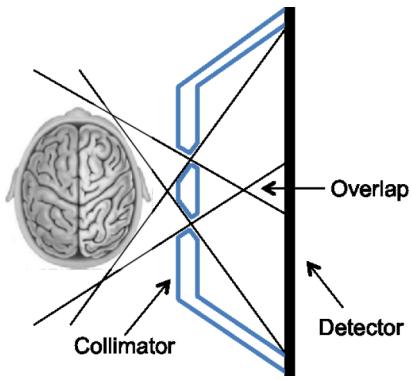

FIG. 5. Overlapping projections in a multiplexing multiple-pinhole system.

multiplexing artifacts.[29,124,125] This indicates that sampling is important, which is confirmed by a study on angular sampling[126] and by another about inconsistent projection data due to truncation.[127] To solve the sampling problem, different groups have successfully combined multiplexed and nonmultiplexed projections. Vunckx *et al.* combined a multiplexing multiple-pinhole collimator with a single pinhole collimator on a dual head camera[29] and Mahmood *et al.* designed a multiple-slit slit-slat collimator with mixed multiplexed and nonmultiplexed projections.[30,31] However, in many multiplexing systems, nonmultiplexed data are already intrinsically available because only a part of the detector is overlapped. In that case, and if the available nonmultiplexed data provide sufficient sampling (also called type I multiplexing in Ref. 27), the acquisition of a separate nonmultiplexed data set is not necessary.[26–28] Moreover, Lin[27,28] also describes type II multiplexing where only a part of the object is sufficiently sampled without multiplexing but its projection data can be used to resolve other parts of the field of view. Van Audenhaege *et al.*[26] extended this with type III multiplexing and showed that the same principle can also be applied to individual sampling angles. When none of these conditions apply, another solution to obtain sufficient data is to obtain a number of projections at different pinhole-detector distances. This approach is known as "synthetic collimation" and was first proposed by Wilson *et al.*[32] and later also applied in the SiliSPECT system[33,34] with two detectors for one collimator, resulting in a nonmultiplexed low-resolution projection and a multiplexed high-resolution projection.

If sufficient data cannot be obtained, it also helps to reduce the solution space by using a body contour to provide prior information during the reconstruction.[29] Sparse activity distributions are also easier to reconstruct from multiplexed data than uniform activity distributions.

While multiplexing provides an increase in sensitivity, a corresponding increase in contrast-to-noise ratio does not necessarily follow in all cases. Reconstructions of multiplexed projection data generally converge more slowly than those of nonmultiplexed data in which case the sensitivity advantage from multiplexing could be essentially irrelevant.[26,128] In this context, the increased sensitivity from multiplexing may only compensate for increased ambiguity.[121] Some groups on the other hand have observed a large increase in the contrast-to-noise ratio when comparing multiplexed with nonmultiplexed setups.[27,31] At first sight, these results seem to contradict the results from Refs. 26, 121, and 128, but interestingly, there is an important difference between these studies, which is related to detector usage. In Refs. 26, 121, and 128, all multiplexed and nonmultiplexed setups use 100% of the detector, while in Refs. 27 and 31, the degree of detector coverage varies between the multiplexed and nonmultiplexed setups (although an approximate correction factor was used in Ref. 31). This might explain the different findings and is supported by Vunckx *et al.*,[121] who stated that once the detector area is entirely used, and the contrast-to-noise ratio does not improve with increased multiplexing. This also explains why reconstructions of sparse activity distributions benefit more from multiplexing than do those of uniform distributions.[128]

More research is needed to fully understand the advantages and disadvantages of multiplexing. For now, we recommend the use of multiplexing mostly for sparse activity distributions and as a way to optimize detector usage. Multiplexing can provide an alternative to other techniques, such as the use of internal shielding or loftholes[90] which have the disadvantage of extra weight and higher manufacturing complexity. As long as the available nonmultiplexed data provide sufficient sampling, no artifacts are to be expected.

2. PRODUCTION TECHNIQUES

Collimator design also involves the practical issues related to manufacturing. Different production methods exist and they all have their specific advantages and disadvantages. Materials that are typically used include lead (Pb), tungsten (W), gold (Au), uranium (U), and platinum (Pt). Because of their cost, Pb and W are by far the most commonly used.

Parallel-, fan-, cone-, and diverging-beam collimators are traditionally fabricated by stamping and stacking lead foils, or by casting molten lead [Fig. 6(a)]. These are relatively easy and cheap techniques, but they have their limitations. As a rule of thumb, the minimum hole diameter is 1.2 mm and the minimum septal thickness is 0.15 mm. These specifications are sufficient for traditional clinical collimators but to build very high-resolution collimators, smaller bores and septa are needed. As an alternative solution, x-ray lithography and metal electroforming allow very high-accuracy collimators to be produced (1 μm) with a variety of metals (e.g., Cu, Ni, Pb, Ag, and Au) [Fig. 7(b)]. It has been demonstrated that 0.025 mm thick gold septa are feasible with this technique.[129] Another technique is based on photochemically etched tungsten foils that were stacked to form the collimator pattern[130] [Fig. 6(b)]. However, the foils need very precise alignment, and the manufacturing precision is limited by the foil thickness.

Pinhole collimators are mostly made from tungsten, which has a higher density than lead (at least in its pure form): 19.3

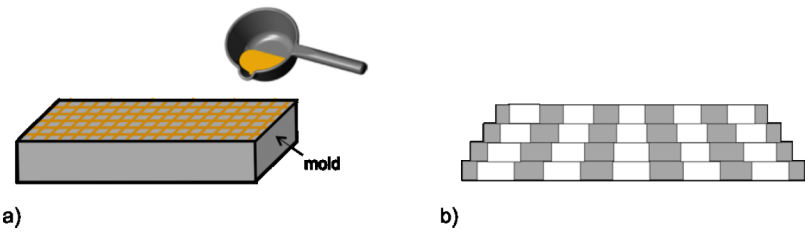

FIG. 6. (a) Lead casting a parallel-hole collimator in a mold (b) stacking tungsten foils to produce a cone-beam collimator.

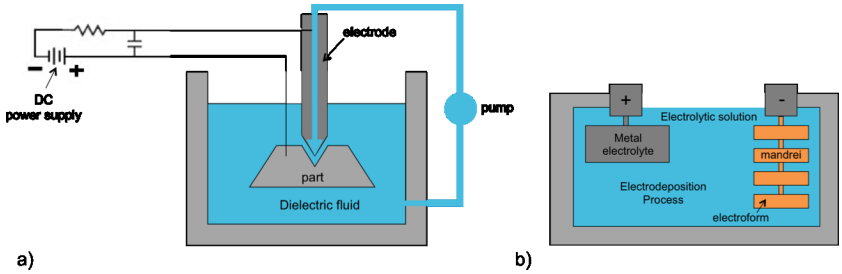

FIG. 7. (a) Electric discharge machining (b) metal electroforming.

versus 11.3 g/cm^3 for pure lead. However, tungsten has a high melting point and cannot be cast like lead. It is also very brittle and difficult to machine. Therefore, one often uses alloys (with nickel, iron, and/or copper) which can then be milled or drilled with a diamond drill, or machined using electric discharge machining (EDM) [Fig. 7(a)]. These techniques are very expensive, and complex shapes like strongly tilted pinholes, loftholes[90] or pinholes with small opening angles cannot be easily produced.

Cold casting is a novel technique based on tungsten powder mixed with epoxy resin. The density of the tungsten composite material is 9 g/cm^3,[131] which is much less than the density of pure tungsten. Therefore, the technique is mostly used for the collimator body, in combination with pinhole inserts made from more dense materials such as tungsten, gold, platinum, uranium, or titanium. In Ref. 131, the pinhole inserts were produced by lost-wax casting a platinum–iridium alloy which results in a density that is even higher than that of gold. This is important because it reduces penetration at the knife-edge, although it was shown that pinhole penetration can largely be compensated for by modeling it in the iterative reconstruction process, unless high-energy radionuclides and very large acceptance angles are used.[91]

Another recent development includes metal additive manufacturing (also referred to as 3D-printing), which can be used to produce complex parts from a 3D computer-aided design (CAD) file.[132] It is based on selective laser melting of tungsten powder that is added in thin layers to build up the desired part (Fig. 8). A density of 18.56 g/cm^3 and a mean deviation of 35 μm were recently reported,[133] and a tungsten parallel-hole collimator was built with a hole size of 525 μm, a septal thickness of 150 μm, and a hole length of 25 mm.[133] This would not be possible with any of the previously described techniques. Moreover, as the material is pure tungsten, it is interesting for building MR-compatible SPECT systems, in contrast to the tungsten alloys that often contain magnetic materials.

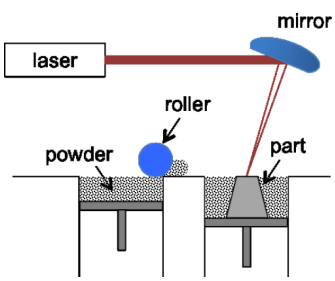

FIG. 8. Additive manufacturing. Powder particles are distributed over the part by the roller. The laser selectively melts certain regions of the powder layer.

3. COLLIMATOR SELECTION

When designing a new system, one of the most important decisions is which collimator to use. Unfortunately, there is no straightforward answer to this question. It depends on the size of the FOV, the intrinsic resolution of the detector, the size of the detector, the target resolution, the energy of the radionuclide being used, the space constraints, and whether the system should be stationary or not.

Pinholes are generally most interesting for imaging small animals because they allow for high magnification so that submillimeter resolutions can be achieved (even with low-resolution detectors). The sensitivity of a single-pinhole collimator is rather low but if the detector is large enough, this can be improved by combining multiple pinholes into a multiple-pinhole collimator. Because the sensitivity decreases quadratically with the distance to the apertures, pinhole collimation was traditionally only interesting for imaging small objects; however, with the emergence of new high-resolution detector technologies, the possibility of using many minifying pinholes allows an increase in sensitivity so that multiple-pinhole imaging also becomes beneficial for medium sized organ imaging (e.g., cerebral and cardiac imaging). Pinholes are also interesting for stationary systems although multiple-slit slit-slat or coded-aperture collimators can also be used for that purpose.

Parallel-hole, fan-beam, and cone-beam collimators have traditionally been the main choice in clinical settings. Parallel-hole collimators have a large FOV and their sensitivity does not decrease with distance, making them very suitable for whole body scanning. Brain SPECT imaging is still most often performed with fan-beam collimation, but cone-beam and slit-slat collimators are also well-suited for medium-size organ or animal imaging.[134] With the emergence of high-resolution detector technologies, we also see new applications, e.g., the use of a fan-beam collimator for small-animal imaging.[135]

If the size and the intrinsic spatial resolution of the detector are known, then we can make an initial selection according to the following algorithm:

1. If the size of the FOV is approximately the same size as that of the detector, then use a parallel-hole, a (multiple-)pinhole, or a (multiple-slit) slit-slat

collimator. The intrinsic resolution of the detector should be better than the desired system (or "target") resolution.
2. If the FOV is larger than the detector, then use a diverging-hole collimator or minifying (multi-)pinhole or (multiple-slit) slit-slat collimator. The intrinsic resolution of the detector should still be better than the target resolution.
3. If the FOV is smaller than the detector, then use a converging beam collimator or magnifying (multiple-)pinhole or (multiple-slit) slit-slat geometry. The intrinsic resolution of the detector needs to be better than the target resolution multiplied by the magnification factor.

The existing literature can also be of great help when selecting a collimator. For example, Goorden *et al.*[20] compared sensitivity and resolution of multiple-pinhole systems based on both high- and low-resolution hemispherical detectors with both a clinical parallel-hole and fan-beam system in the context of clinical brain SPECT imaging. The results are interesting because they show what can be achieved with high-resolution detector technologies compared to clinical parallel-hole and fan-beam systems.

Another interesting comparison was performed for (multiple-slit) slit-slat and parallel-hole collimators[68] for a target resolution of 4, 5, and 10 mm, an intrinsic detector resolution of 3.5 mm, and different FOVs (1–20 cm). It was shown that slit-slat collimators are likely a better choice than parallel-hole for small to medium objects with a long axial field of view.

In Sec. 4.A.1, we also perform a comparison between a cylindrical multiple-pinhole system and a parallel-hole, fan-, and cone-beam system for the same detector surface area, intrinsic resolution, FOV and target resolution.

Collimator selection is easiest if one can assume that the target resolution is known, and then simply maximize the sensitivity. However, choosing the target resolution is not always easy because it depends on the relevant clinical or preclinical imaging task. In 1985, Muehllehner showed with a simulation study that contrast-to-noise ratio increases with resolution, despite the loss in sensitivity. A resolution improvement of 2 mm compensated for a loss in sensitivity by a factor four.[136] Similar results (with a factor of 3) were later found in a measurement study.[137] These studies suggest that, at least for conventional parallel collimation, it may often be advantageous to aim for a high target resolution. On the other hand, there is little doubt that some minimum number of counts is also desirable.[138] Moreover, both of these earlier studies[136,137] were performed using FBP as a reconstruction algorithm. Other studies have suggested a different outcome for the case of iterative reconstruction techniques utilizing resolution recovery, which is mostly used nowadays, and have indicated that it can certainly be useful to re-evaluate the theory. For example, Lau *et al.*[139] showed that when resolution recovery is included, a general-purpose (GP) collimator results in lower noise than a HR collimator for cardiac SPECT, independent of the contrast achieved. Similar results were obtained by Kamphuis *et al.*,[140] who showed that a better contrast-to-noise ratio could be achieved for 2-cm cold lesions in a uniform background when using a GP collimator, rather than a medium-, high-, or ultra-high-resolution collimator. Likewise, McQuaid *et al.*[141] showed that better quantification of 16-mm hot lesions distributed throughout a human torso sized digital phantom could be obtained by using a GP collimator than a HR collimator. Interestingly, Zhou and Gindi found similar results for lesion detectability in an ideal observer study on sinogram data.[142]

4. COLLIMATOR OPTIMIZATION

Collimator optimization should ideally be fully task-dependent, i.e., we wish to compute a metric that describes the task performance for a range of possible values of collimator resolution and allowed septal penetration fraction and then search for where this metric achieves its maximum value. The task metric may be, for example, the channelized Hotelling observer (CHO) signal-to-noise ratio for detection, or the Fisher information for characterizing the uncertainty in the reconstruction, or one of several other possible metrics. We seek to determine the collimator resolution and septal penetration that maximize the given task-based figure-of-merit. But for each possible combination of collimator resolution and septal penetration, we also need to determine an appropriate set of collimator geometric parameters (hole size, hole length, and septal thickness) that will produce the desired resolution and penetration values. The obvious choice is simply to maximize the geometric sensitivity of the collimator. These three constraints then allow one to determine unambiguously the geometric parameters of each collimator for which we need to compute the task performance. Maximizing sensitivity for a certain resolution simply allows one to choose the appropriate set of collimator parameters to accomplish the first step of a full task-dependent optimization.

4.A. Sensitivity maximization for a given target resolution

Once the target resolution is fixed, we need to choose an appropriate set of geometric parameters that will produce the desired resolution and then maximize the sensitivity of the collimator. This problem can be solved analytically for parallel-hole, fan-, and cone-beam collimators but becomes more complicated for multiple-pinhole collimators because of the many degrees of freedom (pinhole aperture, opening angle, number of pinholes, focal length, and radius of rotation). Nevertheless, most optimization methods are ultimately based on the same general procedures:

1. First, decrease the number of degrees of freedom by fixing some design parameters (optional).
2. Next, define subsets of parameters that result in the given target resolution (analytically, if possible, and numerically, otherwise).
3. Finally, determine which of these subsets provide the highest sensitivity. This is the optimal design.

For the target resolution, most optimization papers use the resolution in the center of the FOV, although an average or sensitivity-weighted average resolution has also been used. Furthermore, for this discussion, we have implicitly included effects of collimator penetration within the definition of "target resolution"; however, we recognize that a more general approach can treat resolution and penetration as two different variables that can both affect task performance (e.g., Moore *et al.*[86]).

For the sensitivity, many papers use the point sensitivity in the center of the FOV. However, this might not be the best choice for, e.g., multiple-pinhole collimators where not all pinholes see the complete FOV. In that case, the volume sensitivity, defined as the average point sensitivity for all points in the FOV, is a better choice.

In 1999, Gunter *et al.*[36] described the optimal design of a parallel-hole collimator based on a fixed target resolution and the "University of Chicago Penetration Criterion."[12] Later, Smith *et al.*[143] proposed a slightly different method based on a self-chosen maximum allowable septal-penetration factor and including the finite detector resolution and resolution degradation due to septal penetration.

Gunter *et al.*[36] extended his theory for nonparallel hole collimators (e.g., fan- and cone-beam) by assuming that, locally, these collimator geometries look like parallel-hole designs. This results in fan- and cone-beam collimators that become thinner near the edges. Another approach that results in more conventional fan- and cone-beam collimator designs is presented in Ref. 43. This is based on the same principle of local optimization but it assumes that the optimal collimator thickness and hole diameter are constant and equal to their values near the center of the collimator and that the focal point lies as close as possible behind the object, given the constraint that the FOV must contain the whole body/organ. The optimization was first applied to continuous detectors and then extended to pixelated detectors, with an extra constraint to match the pixels with the collimator holes to improve detector utilization. This was inspired by two earlier optimization studies on matched parallel-hole collimators for scintimammography.[144,145]

As mentioned above, multiple-pinhole collimators are typically more difficult to optimize because of the many degrees of freedom. In most studies, all pinholes are assumed to have the same aperture and focal length but they still need to be positioned (on a ring, a sphere, a flat plate, a helix, etc.) and oriented (e.g., all pointing orthogonally toward the central axis of the system, or focused on the CFOV). To limit the degrees of freedom, most researchers make a few assumptions about the geometry before starting the optimization. For example, Nillius and Danielsson,[61] Goorden and Rentmeester,[20] and Rentmeester *et al.*[146] assume a spherical detector and collimator with all pinholes focusing on the CFOV without truncation. Both Nillius and Danielsson[61] and Goorden and Rentmeester[20] found that the number of pinholes increases faster than the sensitivity decreases due to a larger collimator radius and therefore the optimal system is infinitely large. However, we usually can achieve a sensitivity that is around 95% of the upper bound with a realistic setup. Goorden also showed that this conclusion is only valid for low resolution detectors and that for higher resolution detectors, the system's optimal collimator radius is smaller.[20] Van Holen modified this approach to a cylindrical instead of a spherical geometry[21] and determined the optimal collimator and detector ring radii given the constraint that the detector ring consists of a single ring of predefined flat detectors. In this work, the volume sensitivity, instead of the point sensitivity in the center of the FOV, was considered, as in Ref. 60.

A similar technique was used to optimize a multiple-slit slit-slat collimator for brain imaging,[147] based on point source sensitivity in the center of the FOV.

Finally, it is important to note that high-resolution and high sensitivity are no guarantee for a good image quality. Other important elements that influence image quality include axial sampling sufficiency, angular sampling, penetration, edge effects and scatter, especially for higher energy radionuclides.[148]

4.A.1. Optimized resolution-sensitivity trade-off

As an application of the Sec. 3, we include a comparison between (multiple-) pinhole, parallel-hole, fan-, and cone-beam collimators for two different detector resolutions (0.5 and 3.5 mm) and two different spherical FOVs with a diameter of 30 mm (for small animal applications) and 220 mm (for brain, cardiac, or other organ-specific applications), respectively. We optimized the different collimators by maximizing the volume sensitivity for different target resolutions R_t, given the intrinsic detector resolution, the FOV, the detector size (Table I), and the degree of penetration. Volume sensitivity is defined as the average point sensitivity for all points in the FOV, and target resolutions R_t are defined as the system resolution at the center of the object being imaged. The calculations of the optimal values of volume sensitivity were all based on analytical formulae described in the literature.

1. The parallel-hole optimization was performed based on Eq. (11) from Ref. 143, using 5% septal penetration.
2. The fan- and cone-beam optimizations were based on Ref. 43, also for 5% septal penetration and for a continuous detector but with an adapted formula for calculating the focal length, which is more exact,

TABLE I. Detectors used for the optimization example.

Diameter of the FOV (mm)	Parallel-hole, fan- and cone-beam	Multiple-pinhole
30	3 flat detectors of 7.5×7.5 cm^2	Cylindrical detector with active area of 56.25 cm^2
220	3 flat detectors of 40×40 cm^2	Cylindrical detector with active area of 1600 cm^2

$$f = \frac{z_0}{\cos\left(\pi - \operatorname{atan}\left(\frac{G/2}{z_0 + L_0}\right) - \operatorname{acos}\left(\frac{z_0}{\sqrt{(G/2)^2 + (z_0 + L_0)^2}}\right)\right)} + z_0, \quad (16)$$

with G the detector length, z_0 the point source distance, and L_0 the collimator height, as in the reference paper.[43] So, we looped over different values of L_0, calculated f according to Eq. (16), calculated the hole sizes needed to obtain the target resolution using (2), (3), and (5) from Ref. 43, calculated the volume sensitivity using Eqs. (1), (4), (6), and (7) from Ref. 43, and compared them to find the maximum volume sensitivity.

3. For the multiple-pinhole collimator optimization, we assumed a cylindrical collimator geometry with pinholes arranged along concentrical rings. All pinholes had the same aperture, no axial tilt, and viewed the complete transverse FOV without multiplexing. We optimized the collimator radius c and the detector radius D while keeping the total detector surface area constant and equal to that of the triple head system used for parallel-hole, fan-beam, and cone-beam, by adapting the detector length. So, we looped over different values of c and D and for each combination of c and D:
   - We determined the number of pinholes per ring N_p and their opening angle α using the geometrical relationship that follows from the fact that all pinholes view the complete transverse FOV without allowing overlap of the pinhole projections.
   - We derived the pinhole diameter d needed to achieve the target resolution in the center of the FOV, using Eqs. (10) and (11) and included penetration by using the effective resolution [Eq. (13)]
   - We determined the axial length of the detector ring by dividing the fixed detector surface area by the circumference of the detector ring ($2\pi D$)
   - We calculated volume sensitivity using Eqs. (8) and (9)

Figures 9(a) and 9(b) show sensitivity vs target resolution for a FOV of 220 mm, which corresponds to the size of, e.g., the human brain. The figures show that the cone-beam

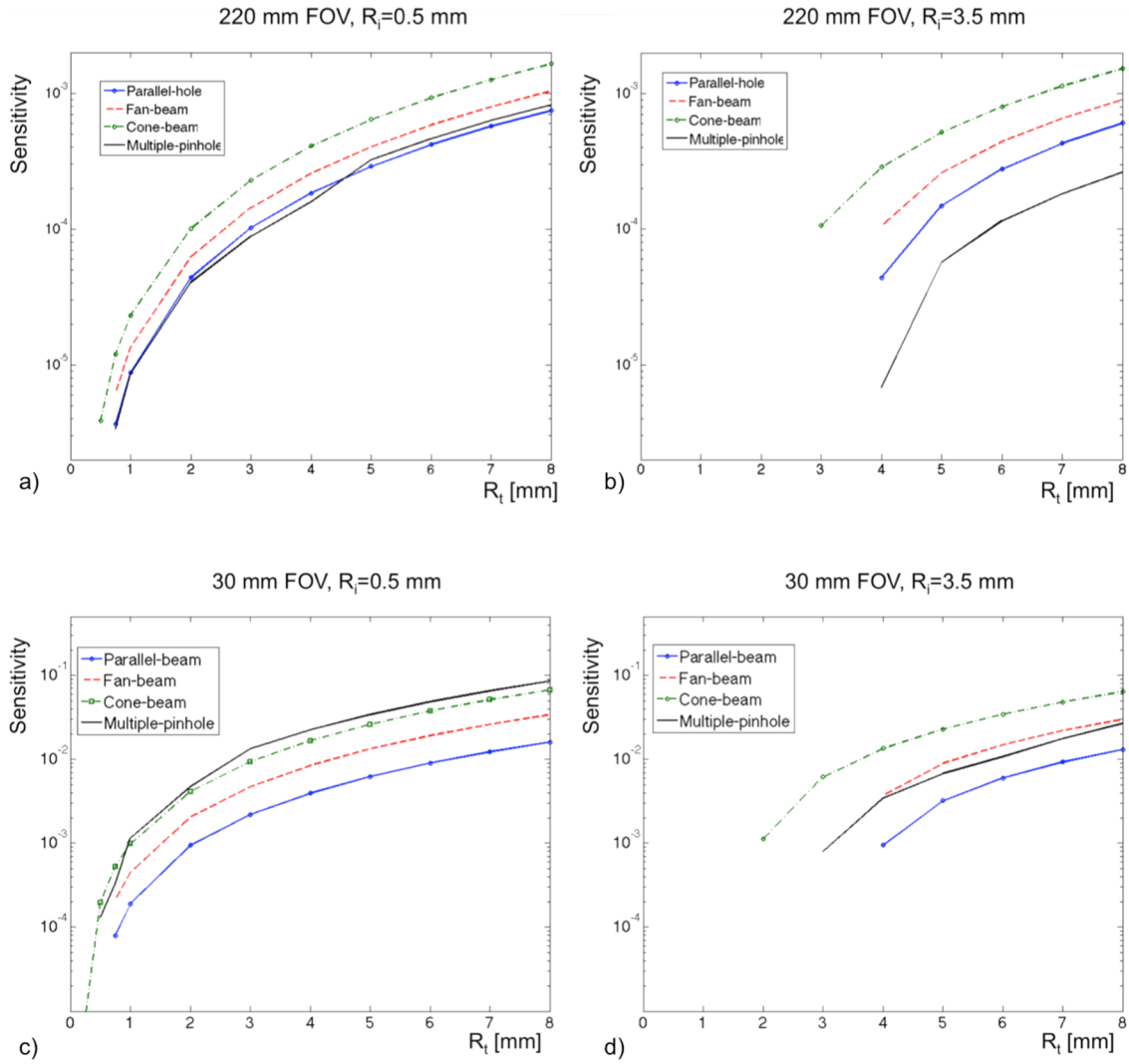

FIG. 9. Sensitivity vs target resolution for (a) a FOV of 220 mm with an intrinsic detector resolution of 0.5 mm (b) a FOV of 220 mm with an intrinsic detector resolution of 3.5 mm (c) a FOV of 30 mm with an intrinsic detector resolution of 0.5 mm (d) a FOV of 30 mm with an intrinsic detector resolution of 3.5 mm.

collimator achieves the highest sensitivity, which is consistent with Park *et al.*[104] We also observe that the cone-beam collimator can achieve the highest target resolution (3 mm for $R_i = 3.5$ and 0.5 mm for $R_i = 0.5$ mm) and that the parallel-hole, fan-, and cone-beam systems do not benefit as much from the high-resolution detector technologies. The multiple-pinhole system, on the other hand, can minify its projections, allowing a higher number of pinholes and thus a higher sensitivity, as shown by Rogulski *et al.*[19]

It is important to note that each graph in Fig. 9 compares different collimators for a certain detector resolution while keeping the detector surface area constant so the conclusion might be different for larger or smaller detectors.

This is also the case for Figs. 9(c) and 9(d) which show sensitivity vs target resolution for a FOV of 30 mm, which corresponds to the size of, e.g., a rat brain. Again, we observe that the multiple-pinhole collimator benefits most from the high-resolution detector. For $R_i = 0.5$ mm, the multiple-pinhole collimator can achieve the highest sensitivity, except when targeting submillimeter resolutions, where it is outperformed by the cone-beam collimator. For the low-resolution detector, the cone-beam is the best choice for all target resolutions. This finding might seem to be at odds with the many commercial small-animal systems, which are all pinhole-based, e.g., the U-SPECT II.[53] However, these systems utilize large clinical triple-head detectors, which need to be placed at a larger distance, and for such a setup, it is not possible to achieve submillimeter resolution with parallel-hole, fan-, or cone-beam collimators. Moreover, most commercial preclinical multiple-pinhole systems have the advantage of being stationary, which can also not be achieved with parallel-hole, fan-, or cone-beam collimators.

4.B. Task-dependent optimization

Ultimately, the goal is to obtain the best possible task performance, regardless of the sensitivity or the resolution of the system. The imaging tasks most relevant to clinical and preclinical SPECT can be broadly classified into two types: (i) lesion-detection tasks and (ii) parameter-estimation tasks. Within each of these categories, there are several different subcategories—for example, detection of lesions in known or unknown locations, or embedded within different types of noisy, structured backgrounds, or estimation of lesion activity concentration, lesion size, and/or local background activity concentration.

While lesion-detection or discrimination perceptual experiments can be performed for collimator optimization—using either receiver-operator characteristic (ROC), or localization ROC, or alternative forced-choice methodologies[149,150]—such studies can be very time-consuming, especially when images from many different collimator-design conditions must be read by multiple observers to determine which design provides the best human-perceptual performance in the diagnostic task being evaluated. For this reason, considerable effort has gone into developing numerical observers of various types.

In 1985, Wagner and Brown reviewed the performance of ideal observers, which attempt to use all of the available image information to calculate a "physical" SNR for any hypothesized lesion.[151] Most observer models compute a decision variable for each of many noisy images; the value of this decision variable is closely related to the likelihood that a lesion is present within a given noisy image. The distribution of decision-variable values when a lesion is known to be present or known to be absent can, in turn, be used to compute the SNR for detection (or detection and localization, or some other relevant diagnostic task). Therefore, it is possible to optimize collimation by maximizing the relevant task SNR, computed using such an ideal observer.

However, the ideal observer operates on the projection data and sets the upper bar for classification performance which may be useful for providing a standard against which the performance of other observers may be compared, but in clinical practice, most tasks are performed using reconstructed images. Therefore, other numerical observers have been developed that operate on reconstructed images.

Observers that have been used for lesion detection include the non-prewhitening observer,[152–154] Hotelling-trace, and CHOs, which have also been shown to correlate well with human observer performance under a variety of different experimental conditions. For example, Fiete *et al.*[155] showed a good correlation between the Hotelling-trace and the human observer for detecting liver tumors, which was later adjusted by Barrett *et al.*[156] who showed that this is only true if the postdetection filtering has a low-pass character and that the channelized Hotelling observer matches better with the human observer. Rolland and Barrett,[157] Eckstein *et al.*,[158] Abbey and Barrett,[159] and Abbey and Barrett,[160] respectively, investigated the effect of a nonuniform background, JPEG image compression, linear iterative reconstruction and noise regularization on different observer models.

For useful reviews of various numerical observers used for assessment of image quality, the reader is referred to Barrett *et al.*,[156] Sharp *et al.*,[153] and Barrett and Myers.[161]

Metrics related to performance in quantitative parameter estimation from images have also been used for collimator optimization. Moore *et al.*[86] evaluated the performance of different medium-energy collimator designs for ^{67}Ga activity estimation by computing a SNR based on the Cramer–Rao lower bound (CRB) on the variance with which tumor activity concentration could be estimated when simultaneously estimating the local background activity concentration. They also showed in this work that the collimator resolution and septal penetration fraction that proved optimal for the activity-estimation task were also close to those that were optimal for lesion detection using the channelized Hotelling observer.

Image reconstruction, itself, can also be considered to be an estimation task in which the goal is to estimate simultaneously all voxel values in the image. Therefore, we can also use the CRB to determine the uncertainty in voxel values to optimize SPECT imaging systems.[162] The calculation of this CRB requires the inversion the Fisher information matrix, which is challenging, certainly for large image volumes, and approximations need to be used. The local shift invariant (LSI) approximation is most commonly used but Fuin *et al.*[162] showed that the conditions for the LSI

approximation are easily violated and described an alternative using a subsampled Fisher information matrix (SFIM). The interested reader is referred to the work of Pato *et al.*,[163] where an overview of different approximation methods and guidelines for a careful choice are given.

Most conventional collimator design studies have optimized the collimation based on the projection data. However, in clinical practice, most imaging tasks are performed using reconstructed images and it has recently been shown that joint optimization of collimation and SPECT reconstruction parameters—as opposed to independent sequential optimization of collimation and reconstruction—yields improved performance, both for lesion-detection tasks[164] and for activity-estimation tasks.[141] The jointly optimized system resolution FWHM was somewhat larger than the average lesion size, consistent with earlier findings of Zeng and Gullberg,[165] and the resolution was further improved by modeling the collimator and detector response function within the iterative reconstruction algorithm.

In both Refs. 164 and 141, the reconstruction parameter being optimized was related to the level of post-reconstruction smoothing but one could also optimize parameters related to the compensation for different image-degrading effects, like the PSF for detector response modeling, factors for attenuation correction [which has been done in time-of-flight PET (Ref. 166)], or geometrical parameters for the collimator model. The geometrical resolution of the collimator is typically modeled using a multiray approach,[167] i.e., not one but multiple rays (sometimes hundreds) are traced from each pixel through the collimator apertures, subsampling the aperture and thus modeling the geometrical resolution of the collimator. For modeling septal penetration and septal scatter effects, one often uses an effective aperture diameter/length or alternatively, in (multiple-)pinhole collimators, aperture penetration can also be modeled using an extended pinhole aperture and more rays for subsampling in order to include rays that might penetrate the pinhole edge.[87]

The distinction between sequential and joint optimization of apertures and reconstruction parameters is not such an important issue for preclinical imaging with multiple-pinhole apertures because such systems are almost never used for planar imaging. Because reconstructed image volumes are always produced, this means that preclinical detection and estimation tasks required by physicians and scientists are generally performed on reconstructed images.

Meng and Clinthorne[168] utilized a modified uniform CRB calculation for optimizing multiple-pinhole collimation. In 2005, Cao *et al.*[125] then used simulated data for optimizing the number of pinholes to use on a single rotating gamma camera for mouse brain imaging. These authors simulated different numbers of pinholes projecting onto a gamma camera (40×40 cm), and multiplexing was allowed. Using a variety of qualitative and quantitative metrics, e.g., the accuracy and precision of the striatum-to-cerebral background ratio, they determined, for this particular camera and scan geometry, that 9 pinholes provided optimal performance. Vunckx *et al.*[169] described an interesting approach, also based on the Fisher information matrix, for optimization of single and multiple pinhole collimators for small-animal SPECT; this method required maximizing a contrast-to-noise ratio computed from the linearized local impulse response and its covariance. Finally, Lee *et al.*[170] numerically optimized a multiple-pinhole collimator for mouse cardiac imaging. These authors considered different numbers of pinholes and different degrees of multiplexed data, for a relatively low-magnification geometry, and they used the CHO to estimate the area under the ROC curve for signal-known-exactly (SKE)/background-known-statistically (BKS) detection of myocardial defects. For a small camera (49×49 mm), these authors determined that the optimal number of pinholes was 4, with the camera rotated by 22.5° about the center of the camera. The optimal magnification factor was 1.52, with 20% multiplexing.

4.C. Adaptive SPECT

In Secs. 4.A and 4.B, we have shown that the optimal collimator not only depends on the detector properties and the size of the FOV (Ref. 110) but also on the detection task,[171] the activity distribution,[119] and the target resolution. These parameters can greatly vary between different patients and scans, and therefore adaptive SPECT systems have been proposed. These systems make it possible, for example, to acquire an initial scout image and then focus on suspicious regions to improve performance.[172] This was first tested with a prototype single pinhole system with an adaptable object-to-pinhole distance, pinhole-to-detector distance, and pinhole aperture sizes.[173] Later, the same group developed an adaptive multiple-pinhole system for small-animal imaging[174,175] with three regions (low, medium, and high magnifications) and adaptable pinhole apertures. The same principle has also been applied to the multiple-slit slit-slat collimator of the C-SPECT cardiac platform using interchangeable slits.[176] The location and size of the heart is first estimated during a scout scan to increase the image quality of the actual image acquisition. Another interesting application is described by Li and Meng[119] and Fuin *et al.*[162] who used adaptive angular sampling, i.e., they optimized the time spent at each angle depending on the activity distribution.

5. CONCLUDING DISCUSSION

In the last several years, there has been tremendous progress on many collimation-related topics, for both human and small-animal molecular imaging systems. Many new detectors have become available with greatly improved intrinsic spatial resolution; these call for the use of diverging and minifying collimators and change the requirements for optimal collimation. New production techniques have also become available (e.g., direct 3-D printing of metals and "cold casting" of tungsten-composite materials) opening up new possibilities for fabrication of complex new collimator designs that would be impossible or extremely expensive to construct by more conventional means. There has also been good progress recently on fully stationary SPECT systems based on ingenious collimator and detector designs. These offer potential advantages for dynamic scanning, for improved

system stability, and for compatibility with MRI, enabling the development of truly simultaneous SPECT/MR scanners.

In addition to reviewing recent advances in collimator technology, we have also provided here useful guidelines for optimizing a SPECT collimator for a specific imaging task and discussed the necessary sampling conditions needed for reconstructing data from stationary systems or multiplexed multiple-pinhole SPECT systems.

ACKNOWLEDGMENTS

This work was supported by Ghent University (Multidisciplinary Research Partnership: The integrative neuroscience of behavioural control), iMinds Medical IT, and the Research Foundation Flanders (FWO, Belgium). Karen Van Audenhaege is supported by a doctoral fellowship of the agency for Innovation by Science and Technology (IWT) and Roel Van Holen is supported by a postdoctoral fellowship of the Research Foundation Flanders (FWO). Christian Vanhove is supported by the GROUP-ID consortium of Ghent University. Scott D. Metzler and Stephen C. Moore are supported by the National Heart, Lung, and Blood Institute (NHLBI) of the National Institutes of Health under Grant No. R01-HL-111883. S. D. Metzler is also supported by NHLBI under Grant No. R01-HL-108119.

[a]Author to whom correspondence should be addressed. Electronic mail: karen.vanaudenhaege@ugent.be

[1]O. Chiewitz and G. Hevesy, "Radioactive indicators in the study of phosphorous metabolism in rats," Nature **136**, 754–755 (1935).
[2]G. Mariani and H. W. Strauss, "Positron emission and single-photon emission imaging: Synergy rather than competition," Eur. J. Nucl. Med. Mol. Imaging **38**, 1189–1190 (2011).
[3]G. Mariani, L. Bruselli, T. Kuwert, E. E. Kim, A. Flotats, O. Israel, M. Dondi, and N. Watanabe, "A review on the clinical uses of SPECT/CT," Eur. J. Nucl. Med. Mol. Imaging **37**, 1959–1985 (2010).
[4]A. K. Paul and H. A. Nabi, "Gated myocardial perfusion SPECT: Basic principles, technical aspects, and clinical applications," J. Nucl. Med. Technol. **32**, 179–187 (2004).
[5]M. Horger and R. Bares, "The role of single-photon emission computed tomography/computed tomography in benign and malignant bone disease," Semin. Nucl. Med. **36**, 286–294 (2006).
[6]D. J. Kwekkeboom, H. van Urk, B. K. Pauw, S. W. Lamberts, P. P. Kooij, R. P. Hoogma, and E. P. Krenning, "Octreotide scintigraphy for the detection of paragangliomas," J. Nucl. Med. **34**, 873–878 (1993).
[7]G. L. Zeng, J. R. Galt, M. N. Wernick, R. A. Mintzer, and J. N. Aarsvold, "Single-photon emission computed tomography," in *Emission Tomography: The Fundamentals of PET and SPECT* (Elsevier Academic, San Diego, London, 2004), Chap. 7, pp. 127–151.
[8]S. M. Lim, A. Katsifis, V. L. Villemagne, R. Best, G. Jones, M. Saling, J. Bradshaw, J. Merory, M. Woodward, M. Hopwood, and C. C. Rowe, "The 18F-FDG PET cingulate island sign and comparison to 123I-beta-CIT SPECT for diagnosis of dementia with Lewy bodies," J. Nucl. Med. **50**, 1638–1645 (2009).
[9]M. Ichise, H. Toyama, L. Fornazzari, J. R. Ballinger, and J. C. Kirsh, "Iodine-123-IBZM dopamine D2 receptor and technetium-99m-HMPAO brain perfusion SPECT in the evaluation of patients with and subjects at risk for Huntington's disease," J. Nucl. Med. **34**, 1274–1281 (1993).
[10]S. R. Meikle, P. Kench, M. Kassiou, and R. B. Banati, "Small animal SPECT and its place in the matrix of molecular imaging technologies," Phys. Med. Biol. **50**, R45–R61 (2005).
[11]S. Moore, K. Kouris, and I. Cullum, "Collimator design for single photon emission tomography," Eur. J. Nucl. Med. **19**, 138–150 (1992).
[12]D. L. Gunter, "Collimator design for nuclear medicine," in *Emission Tomography: The Fundamentals of PET and SPECT* (Elsevier Academic, San Diego, London, 2004), Chap. 8, pp. 153–168.
[13]S. R. Meikle, P. L. Kench, and J. Lin, "Design considerations of small-animal SPECT cameras," in *Molecular Imaging of Small Animals–Instrumentation and Applications*, edited by H. Zaidi (Springer, Geneva, Switzerland, 2014).
[14]D. R. Schaart, H. T. van Dam, S. Seifert, R. Vinke, P. Dendooven, H. Löhner, and F. J. Beekman, "A novel, SiPM-array-based, monolithic scintillator detector for PET," Phys. Med. Biol. **54**, 3501–3512 (2009).
[15]M. Georgiou, G. Borghi, S. V. Spirou, G. Loudos, and D. R. Schaart, "First performance tests of a digital photon counter (DPC) array coupled to a CsI(Tl) crystal matrix for potential use in SPECT," Phys. Med. Biol. **59**, 2415–2430 (2014).
[16]C. Bouckaert, S. Vandenberghe, and R. Van Holen, "Evaluation of a compact, high-resolution SPECT detector based on digital silicon photomultipliers," Phys. Med. Biol. **59**, 7521–7539 (2014).
[17]H. B. Barber, H. H. Barrett, F. L. Augustine, W. J. Hamilton, B. A. Apotovsky, E. L. Dereniak, F. P. Doty, J. D. Eskin, J. P. Garcia, D. G. Marks, K. J. Matherson, J. M. Woolfenden, and E. T. Young, "Development of a 64 × 64 CdZnTe array and associated readout integrated circuit for use in nuclear medicine," J. Electron. Mater. **26**, 765–772 (1997).
[18]T. E. Peterson and L. R. Furenlid, "SPECT detectors: The Anger camera and beyond," Phys. Med. Biol. **56**, R145–R182 (2011).
[19]M. Rogulski, H. Barber, H. Barrett, R. Shoemaker, and J. Woolfenden, "Ultra-high-resolution brain SPECT imaging: Simulation results," IEEE Trans. Nucl. Sci. **40**, 1123–1129 (1993).
[20]M. C. Goorden, M. C. M. Rentmeester, and F. J. Beekman, "Theoretical analysis of full-ring multi-pinhole brain SPECT," Phys. Med. Biol. **54**, 6593–6610 (2009).
[21]R. Van Holen, B. Vandeghinste, K. Deprez, and S. Vandenberghe, "Design and performance of a compact and stationary microSPECT system," Med. Phys. **40**, 112501 (11pp.) (2013).
[22]D. Meier, D. J. Wagenaar, S. Chen, J. Xu, J. Yu, and B. M. W. Tsui, "A SPECT camera for combined MRI and SPECT for small animals," Nucl. Instrum. Methods Phys. Res., Sect. A **652**, 731–734 (2011).
[23]M. J. Hamamura, S. Ha, W. W. Roeck, L. T. Muftuler, D. J. Wagenaar, D. Meier, B. E. Patt, and O. Nalcioglu, "Development of an MR-compatible SPECT system (MRSPECT) for simultaneous data acquisition," Phys. Med. Biol. **55**, 1563–1575 (2010).
[24]L. Cai, X. Lai, Z. Shen, C.-T. Chen, and L.-J. Meng, "MRC-SPECT: A sub- 500 μm resolution MR-compatible SPECT system for simultaneous dual-modality study of small animals," Nucl. Instrum. Methods Phys. Res., Sect. A **734**, 147–151 (2014).
[25]P. Busca, C. Fiorini, A. D. Butt, M. Occhipinti, R. Peloso, R. Quaglia, F. Schembari, P. Trigilio, G. Nemeth, P. Major, K. Erlandsson, and B. F. Hutton, "Simulation of the expected performance of INSERT: A new multimodality SPECT/MRI system for preclinical and clinical imaging," Nucl. Instrum. Methods Phys. Res., Sect. A **734**, 141–146 (2014).
[26]K. Van Audenhaege, C. Vanhove, S. Vandenberghe, and R. Van Holen, "The evaluation of data completeness and image quality in multiplexing multi-pinhole SPECT," IEEE Trans. Med. Imaging **34**, 474–486 (2014).
[27]J. Lin, "On artifact-free projection overlaps in multi-pinhole tomographic imaging," IEEE Trans. Med. Imaging **32**, 2215–2229 (2013).
[28]J. Lin, "An extension to artifact-free projection overlaps," Med. Phys. **42**, 2179–2193 (2015).
[29]K. Vunckx, J. Nuyts, B. Vanbilloen, M. De Saint-hubert, D. Vanderghinste, D. Rattat, F. M. Mottaghy, and M. Defrise, "Optimized multipinhole design for mouse imaging," IEEE Trans. Nucl. Sci. **56**, 2696–2705 (2009).
[30]S. T. Mahmood, K. Erlandsson, I. Cullum, and B. F. Hutton, "The potential for mixed multiplexed and non-multiplexed data to improve the reconstruction quality of a multi-slit-slat collimator SPECT system," Phys. Med. Biol. **55**, 2247–2268 (2010).
[31]S. Mahmood, K. Erlandsson, I. Cullum, and B. Hutton, "Experimental results from a prototype slit-slat collimator with mixed multiplexed and non-multiplexed data," Phys. Med. Biol. **56**, 4311–4331 (2011).
[32]D. W. Wilson, H. H. Barrett, and E. W. Clarkson, "Reconstruction of two- and three-dimensional images from synthetic-collimator data," IEEE Trans. Med. Imaging **19**, 412–422 (2000).
[33]S. Shokouhi, S. D. Metzler, D. W. Wilson, and T. E. Peterson, "Multi-pinhole collimator design for small-object imaging with SiliSPECT: A high-resolution SPECT," Phys. Med. Biol. **54**, 207–225 (2009).
[34]S. Shokouhi, D. W. Wilson, S. D. Metzler, and T. E. Peterson, "Evaluation of image reconstruction for mouse brain imaging with synthetic collimation from highly multiplexed SiliSPECT projections," Phys. Med. Biol. **55**, 5151–5168 (2010).

[35]H. O. Anger, "Scintillation camera with multichannel collimators," J. Nucl. Med. **5**, 515–531 (1964).
[36]D. Gunter, K. Matthews, and C. Ordoñez, "The optimal design of non-parallel hole collimators," in *IEEE Nuclear Science Symposium Conference Record* (IEEE, Seattle, WA, 1999), Vol. 3, pp. 1344–1348.
[37]H. Wieczorek and A. Goedicke, "Analytical model for SPECT detector concepts," IEEE Trans. Nucl. Sci. **53**, 1102–1112 (2006).
[38]R. L. Mather, "Gamma-ray collimator penetration and scattering effects," J. Appl. Phys. **28**, 1200–1207 (1957).
[39]M. S. Gerber and D. W. Miller, "Parallel-hole collimator design," J. Nucl. Med. **15**, 724–725 (1974).
[40]R. A. Moyer, "A low-energy multihole converging collimator compared with a pinhole collimator," J. Nucl. Med. **15**, 59–64 (1974).
[41]A. R. Formiconi, "Geometrical response of multihole collimators," Phys. Med. Biol. **43**, 3359–3379 (1998).
[42]M. Park, M. Kijewski, and S. Moore, "Effects of hole tapering on cone-beam collimation for brain SPECT imaging," Nucl. Instrum. Methods Phys. Res., Sect. A **569**, 188–192 (2006).
[43]R. M. Capote, N. Matela, R. C. Conceição, and P. Almeida, "Optimization of convergent collimators for pixelated SPECT systems," Med. Phys. **40**, 062501 (13pp.) (2013).
[44]G. Muehllehner, "A diverging collimator for gamma-ray imaging cameras," J. Nucl. Med. **10**, 197–201 (1969).
[45]L. Moerman, D. De Naeyer, P. Boon, and F. De Vos, "P-glycoprotein at the blood-brain barrier: Kinetic modeling of 11C-desmethylloperamide in mice using a 18F-FDG μPET scan to determine the input function," Eur. J. Nucl. Med. Mol. Imaging Res. **1**, 1–9 (2011).
[46]K. Ogawa and M. Muraishi, "Feasibility study on an ultra-high-resolution SPECT with CdTe detectors," IEEE Trans. Nucl. Sci. **57**, 17–24 (2010).
[47]M. Smith, R. Jaszczak, and H. Wang, "Pinhole aperture design for ^{131}I tumor imaging," IEEE Trans. Nucl. Sci. **44**, 1154–1160 (1997).
[48]J. Lin and S. R. Meikle, "SPECT using asymmetric pinholes with truncated projections," Phys. Med. Biol. **56**, 4103–4118 (2011).
[49]M. C. Goorden and F. J. Beekman, "High-resolution tomography of positron emitters with clustered pinhole SPECT," Phys. Med. Biol. **55**, 1265–1277 (2010).
[50]D. Paix, "Pinhole imaging of gamma rays," Phys. Med. Biol. **12**, 489–500 (1967).
[51]S. D. Metzler, J. E. Bowsher, M. F. Smith, and R. J. Jaszczak, "Analytic determination of pinhole collimator sensitivity with penetration," IEEE Trans. Med. Imaging **20**, 730–741 (2001).
[52]R. Accorsi and S. D. Metzler, "Analytic determination of the resolution-equivalent effective diameter of a pinhole collimator," IEEE Trans. Med. Imaging **23**, 750–763 (2004).
[53]F. Van Der Have, B. Vastenhouw, R. M. Ramakers, W. Branderhorst, J. O. Krah, C. Ji, S. G. Staelens, and F. J. Beekman, "U-SPECT-II: An ultra-high-resolution device for molecular small-animal imaging," J. Nucl. Med. **50**, 599–605 (2009).
[54]B. W. Miller, L. R. Furenlid, S. K. Moore, H. B. Barber, V. V. Nagarkar, and H. H. Barrett, "System integration of FastSPECT III, a dedicated SPECT rodent-brain imager based on BazookaSPECT detector technology," in *IEEE Nuclear Science Symposium Conference Record* (IEEE, Orlando, FL, 2009), pp. 4004–4008.
[55]K. Lin, I.-T. Hsiao, C. Wietholt, Y. Chung, C. Chen, and Y. T, "Performance evaluation of an animal SPECT using modified NEMA standards," J. Nucl. Med. **49**, 402P (2008).
[56]N. Schramm, G. Ebel, U. Engeland, T. Schurrat, M. Behe, and T. Behr, "High-resolution SPECT using multipinhole collimation," IEEE Trans. Nucl. Sci. **50**, 315–320 (2003).
[57]W. Chang, C. E. Ordonez, H. Liang, Y. Li, and J. Liu, "C-SPECT a clinical cardiac SPECT/CT platform: Design concepts and performance potential," IEEE Trans. Nucl. Sci. **56**, 2659–2671 (2009).
[58]J. Dey, "Improvement of performance of cardiac SPECT camera using curved detectors with pinholes," IEEE Trans. Nucl. Sci. **59**, 334–347 (2012).
[59]T. Funk, D. Kirch, J. Koss, E. Botvinick, and B. Hasegawa, "A novel approach to multipinhole SPECT for myocardial perfusion imaging," J. Nucl. Med. **47**, 595–602 (2006).
[60]K. Van Audenhaege, S. Vandenberghe, K. Deprez, B. Vandeghinste, and R. Van Holen, "Design and simulation of a full-ring multi-lofthole collimator for brain SPECT," Phys. Med. Biol. **58**, 6317–6336 (2013).
[61]P. Nillius and M. Danielsson, "Theoretical bounds and system design for multipinhole SPECT," IEEE Trans. Med. Imaging **29**, 1390–1400 (2010).
[62]B. J. Min, Y. Choi, N.-Y. Lee, K. Lee, Y. B. Ahn, and J. Joung, "Design consideration of a multipinhole collimator with septa for ultra high-resolution silicon drift detector modules," Nucl. Instrum. Methods Phys. Res., Sect. A **606**, 755–761 (2009).
[63]F. Garibaldi, R. Accorsi, M. Cinti, E. Cisbani, S. Colilli, F. Cusanno, G. De Vincentis, A. Fortuna, R. Fratoni, B. Girolami, F. Ghio, F. Giuliani, M. Gricia, R. Lanza, A. Loizzo, S. Loizzo, M. Lucentini, S. Majewski, F. Santavenere, R. Pani, R. Pellegrini, A. Signore, F. Scopinaro, and P. Veneroni, "Small animal imaging by single photon emission using pinhole and coded aperture collimation," IEEE Trans. Nucl. Sci. **52**, 573–579 (2005).
[64]R. Accorsi, F. Gasparini, and R. C. Lanza, "Optimal coded aperture patterns for improved SNR in nuclear medicine imaging," Nucl. Instrum. Methods Phys. Res., Sect. A **474**, 273–284 (2001).
[65]S. R. Meikle, P. Kench, A. G. Weisenberger, R. Wojcik, M. F. Smith, S. Majewski, S. Eberl, R. R. Fulton, A. B. Rosenfeld, and M. J. Fulham, "A prototype coded aperture detector for small animal SPECT," IEEE Nucl. Sci. Symp. Conf. Rec. **3**, 1580–1584 (2001).
[66]S. R. Meikle, R. Wojcik, A. G. Weisenberger, M. F. Smith, S. Majewski, P. Kench, S. Eberl, R. R. Fulton, M. Lerch, and A. B. Rosenfeld, "CoALA-SPECT: A coded aperture laboratory animal SPECT system for pre clinical imaging," IEEE Nucl. Sci. Symp. Conf. Rec. **2**, 1061–1065 (2002).
[67]R. Accorsi, J. R. Novak, A. S. Ayan, and S. D. Metzler, "Derivation and validation of a sensitivity formula for slit-slat collimation," IEEE Trans. Med. Imaging **27**, 709–722 (2008).
[68]S. D. Metzler, R. Accorsi, A. S. Ayan, and R. J. Jaszczak, "Slit-slat and multi-slit-slat collimator design and experimentally acquired phantom images from a rotating prototype," IEEE Trans. Nucl. Sci. **57**, 125–134 (2010).
[69]G. L. Zeng, D. Gagnon, C. G. Matthews, J. A. Kolthammer, J. D. Radachy, and W. G. Hawkins, "Image reconstruction algorithm for a rotating slat collimator," Med. Phys. **29**, 1406–1412 (2002).
[70]S. Vandenberghe, R. Van Holen, S. Staelens, and I. Lemahieu, "System characteristics of SPECT with a slat collimated strip detector," Phys. Med. Biol. **51**, 391–405 (2006).
[71]R. Van Holen, S. Vandenberghe, S. Staelens, and I. Lemahieu, "Comparing planar image quality of rotating slat and parallel hole collimation: Influence of system modeling," Phys. Med. Biol. **53**, 1989–2002 (2008).
[72]R. Van Holen, "SPECT imaging with rotating slat collimation," Ph.D. thesis, University Ghent, 2009.
[73]L. Zhou, K. Vunckx, and J. Nuyts, "Parallel hole and rotating slat collimators: Comparative study using digital contrast phantoms," IEEE Trans. Nucl. Sci. **60**, 3282–3289 (2013).
[74]R. Clack, P. Christian, M. Defrise, and A. E. Welch, "Image reconstruction for a novel SPECT system with rotating slant-hole collimators," IEEE Nucl. Sci. Symp. Conf. Rec. **4**, 1948–1952 (1994).
[75]C. Liu, J. Xu, and B. M. W. Tsui, "Myocardial perfusion SPECT using a rotating multi-segment slant-hole collimator," Med. Phys. **37**, 1610–1618 (2010).
[76]G. Bal, E. V. R. DiBella, G. T. Gullberg, and G. L. Zeng, "Cardiac imaging using a four-segment slant-hole collimator," IEEE Trans. Nucl. Sci. **53**, 2619–2627 (2006).
[77]R. H. Moore, N. M. Alpert, and H. W. Strauss, "A variable angle slant-hole collimator," J. Nucl. Med. **24**, 61–65 (1983).
[78]C. Liu, J. Xu, and B. Tsui, "Development and evaluation of rotating multi-segment variable-angle slant-hole spect," Soc. Nucl. Med. Annu. Meet. Abstr. **48**, 161P (2007).
[79]Z. Cao and B. Tsui, "An analytical reconstruction algorithm for multifocal converging-beam SPECT," Phys. Med. Biol. **39**, 281–291 (1994).
[80]P. C. Hawman and E. J. Haines, "The cardiofocal collimator: A variable-focus collimator for cardiac SPECT," Phys. Med. Biol. **39**, 439–450 (1994).
[81]M. A. Park, M. F. Kijewski, L. Horky, M. Keijzers, R. Keijzers, L. Kalfin, J. Crough, M. Goswami, and S. C. Moore, "Fabrication and calibration of a novel high-sensitivity collimator for brain SPECT imaging," in *Annual Meeting of the American Association of Physicists in Medicine (AAPM)* (Medical Physics, Austin, TX, 2014), Vol. 41, presentation SU-C-9A-7.
[82]S. C. Moore, M. F. Kijewski, M. Cervo, C. Mauceri, L. Horky, and M. A. Park, "Reconstruction of brain SPECT data from an ultra-short cone-beam collimator paired with a fan-beam collimator," in *Proceedings, Fully Three-Dimensional Image Reconstruction in Radiology and Nuclear Medicine*, *Newport, RI* (2015), paper 40.
[83]P. Mi-Ae, S. C. Moore, and M. F. Kijewski, "System and method for performing Single Photon Emission Computed Tomography (SPECT) with

a focal-length cone-beam collimation," U.S. patent 20080302950 A1 (Dec. 11, 2008).
[84]S. Cherry, J. Sorenson, and M. Phelps, *Physics in Nuclear Medicine*, 3rd ed. (Saunders, 1987), pp. 239–240.
[85]E. Keller, "Optimum dimensions of parallel-hole, multi-aperture collimators for gamma-ray cameras," J. Nucl. Med. **9**, 233–235 (1968).
[86]S. Moore, M. Kijewski, and G. E. Fakhri, "Collimator optimization for detection and quantitation tasks: Application to gallium-67 imaging," IEEE Trans. Med. Imaging **24**, 1347–1356 (2005).
[87]M. Gieles, H. W. A. M. de Jong, and F. J. Beekman, "Monte Carlo simulations of pinhole imaging accelerated by kernel-based forced detection," Phys. Med. Biol. **47**, 1853–1867 (2002).
[88]M. F. Smith and R. J. Jaszczak, "An analytic model of pinhole aperture penetration for 3D pinhole SPECT image reconstruction," Phys. Med. Biol. **43**, 761–775 (1998).
[89]F. Van Der Have and F. Beekman, "Penetration, scatter and sensitivity in channel micro-pinholes for SPECT: A Monte Carlo investigation," IEEE Trans. Nucl. Sci. **53**, 2635–2645 (2006).
[90]K. Deprez, L. Pato, R. Van Holen, and S. Vandenberghe, "Characterization of a SPECT pinhole collimator for optimal detector usage (the lofthole)," Phys. Med. Biol. **58**, 859–885 (2013).
[91]V. Bom, M. Goorden, and F. Beekman, "Comparison of pinhole collimator materials based on sensitivity equivalence," Phys. Med. Biol. **56**, 3199–3214 (2011).
[92]R. Van Holen, S. Staelens, and S. Vandenberghe, "SPECT imaging of high energy isotopes and isotopes with high energy contaminants with rotating slat collimators," Med. Phys. **36**, 4257–4267 (2009).
[93]S. Walrand, M. Hesse, R. Wojcik, R. Lhommel, and F. Jamar, "Optimal design of Anger camera for bremsstrahlung imaging: Monte Carlo evaluation," Front. Oncol. **4**, 149 (7pp.) (2014).
[94]I. Perali, A. Celani, L. Bombelli, C. Fiorini, F. Camera, E. Clementel, S. Henrotin, G. Janssens, D. Prieels, F. Roellinghoff, J. Smeets, F. Stichelbaut, and F. V. Stappen, "Prompt gamma imaging of proton pencil beams at clinical dose rate," Phys. Med. Biol. **59**, 5849–5871 (2014).
[95]S. Orlov, "Theory of three-dimensional reconstruction. II. The recovery operator," Sov. Phys. - Crystallogr. **20**, 429–433 (1975).
[96]H. K. Tuy, "An inversion formula for cone-beam reconstruction," SIAM J. Appl. Math. **43**, 546–552 (1983).
[97]B. D. Smith, "Image reconstruction from cone-beam projections: Necessary and sufficient conditions and reconstruction methods," IEEE Trans. Med. Imaging **4**, 14–25 (1985).
[98]J. Li, R. J. Jaszczak, A. Van Mullekom, C. Scarfone, K. L. Greer, and R. E. Coleman, "Half-cone beam collimation for triple-camera SPECT systems," J. Nucl. Med. **37**, 498–502 (1996).
[99]R. K. Rowe, J. N. Aarsvold, H. H. Barrett, J. C. Chen, W. P. Klein, B. A. Moore, I. W. Pang, D. D. Patton, and T. A. White, "A stationary hemispherical SPECT imager for three-dimensional brain imaging," J. Nucl. Med. **34**, 474–480 (1993).
[100]C. Stone, M. Smith, K. Greer, and R. Jaszczak, "A combined half-cone beam and parallel hole collimation system for SPECT brain imaging," IEEE Trans. Nucl. Sci. **45**, 1219–1224 (1998).
[101]R. J. Jaszczak, J. Li, H. Wang, and R. E. Coleman, "Three-dimensional SPECT reconstruction of combined cone beam and parallel beam data," Phys. Med. Biol. **37**, 535–548 (1992).
[102]G. L. Zeng, "Revisit of combined parallel-beam/cone-beam or fan-beam/cone-beam imaging," Med. Phys. **40**, 100701 (5pp.) (2013).
[103]G. T. Gullberg and G. L. Zeng, "Three-dimensional SPECT reconstruction of combined conebeam and fan-beam data acquired using a three-detector SPECT system," in *Proceedings, Fully Three-Dimensional Image Reconstruction in Radiology and Nuclear Medicine* (Springer, Aix-les-Bains, Savoie, France, 1995), p. 329.
[104]M. Park, S. Moore, and M. Kijewski, "Brain SPECT with short focal-length cone-beam collimation," Med. Phys. **32**, 2236–2244 (2005).
[105]R. J. Jaszczak, K. L. Greer, J. E. Bowsher, S. D. Metzler, R. Ter-Antonyan, and K. V. Bobkov, "Helical-path, half-cone-beam acquisition for SPECT brain imaging," IEEE Nucl. Sci. Conf. Rec. **3**, 1837–1841 (2006).
[106]R. Ter-Antonyan, R. J. Jaszczak, J. E. Bowsher, K. L. Greer, and S. D. Metzler, "Brain SPECT simulation using half-cone-beam collimation and single-revolution helical-path acquisition," IEEE Trans. Nucl. Sci. **54**, 475–479 (2007).
[107]G. L. Zeng, "Helical SPECT using axially truncated data," IEEE Trans. Nucl. Sci. **46**, 2111–2118 (1999).
[108]S. Metzler, K. Greer, and R. Jaszczak, "Helical pinhole SPECT for small-animal imaging: A method for addressing sampling completeness," IEEE Trans. Nucl. Sci. **50**, 1575–1583 (2003).
[109]P. E. B. Vaissier, M. C. Goorden, B. Vastenhouw, F. van der Have, R. M. Ramakers, and F. J. Beekman, "Fast spiral SPECT with stationary γ-cameras and focusing pinholes," J. Nucl. Med. **53**, 1292–1299 (2012).
[110]G. S. P. Mok, J. Yu, Y. Du, Y. Wang, and B. M. W. Tsui, "Evaluation of a multi-pinhole collimator for imaging small animals with different sizes," Mol. Imaging Biol. **14**, 60–69 (2012).
[111]C. Vanhove, M. Defrise, T. Lahoutte, and A. Bossuyt, "Three-pinhole collimator to improve axial spatial resolution and sensitivity in pinhole SPECT," Eur. J. Nucl. Med. Mol. Imaging **35**, 407–415 (2008).
[112]C. Lackas, N. Schramm, J. Hoppin, U. Engeland, A. Wirrwar, and H. Halling, "T-SPECT: A novel imaging technique for small animal research," IEEE Trans. Nucl. Sci. **52**, 181–187 (2005).
[113]S. D. Metzler, J. E. Bowsher, and R. J. Jaszczak, "Geometrical similarities of the Orlov and Tuy sampling criteria and a numerical algorithm for assessing sampling completeness," IEEE Nucl. Sci. Conf. Rec. **50**, 1241–1245 (2002).
[114]R. J. Jaszczak, J. Li, H. Wang, M. R. Zalutsky, and R. E. Coleman, "Pinhole collimation for ultra-high-resolution, small-field-of-view SPECT," Phys. Med. Biol. **39**, 425–437 (1994).
[115]C. Shannon, "Communication in the presence of noise," Proc. IRE **37**, 10–21 (1949).
[116]B. F. Hutton, "Angular sampling necessary for clinical SPECT," J. Nucl. Med. **37**, 1915–1916 (1996).
[117]J. A. Bieszk and E. G. Hawman, "Evaluation of SPECT angular sampling effects: Continuous versus step-and-shoot acquisition," J. Nucl. Med. **28**, 1308–1314 (1987).
[118]Z. Cao, L. E. Holder, and C. C. Chen, "Optimal number of views in 360 degrees SPECT imaging," J. Nucl. Med. **37**, 1740–1744 (1996).
[119]N. Li and L.-J. Meng, "Adaptive angular sampling for SPECT imaging," IEEE Trans. Nucl. Sci. **58**, 2205–2218 (2011).
[120]S. C. Moore, M. MacKnight, M.-A. Park, and R. E. Zimmerman, "Reduction of micro-SPECT streak artifacts from imperfect system modeling," IEEE Nucl. Sci. Symp. Conf. Rec. **5**, 3361–3363 (2007).
[121]K. Vunckx, P. Suetens, and J. Nuyts, "Effect of overlapping projections on reconstruction image quality in multipinhole SPECT," IEEE Trans. Med. Imaging **27**, 972–983 (2008).
[122]K. Parnham, S. Chowdhury, J. Li, D. Wagenaar, and B. Patt, "Second-generation, tri-modality pre-clinical imaging system," IEEE Nucl. Sci. Conf. Rec. **3**, 1802–1805 (2006).
[123]S. Deleye, R. Van Holen, J. Verhaeghe, S. Vandenberghe, S. Stroobants, and S. Staelens, "Performance evaluation of small-animal multipinhole μSPECT scanners for mouse imaging," Eur. J. Nucl. Med. Mol. Imaging **40**, 744–758 (2013).
[124]F. P. Difilippo and S. Patel, "Strategies to reduce artifacts and improve accuracy in multiplexed multi-pinhole small animal SPECT," IEEE Nucl. Sci. Conf. Rec. **1**, 3151–3154 (2009).
[125]Z. Cao, G. Bal, R. Accorsi, and P. Acton, "Optimal number of pinholes in multi-pinhole SPECT for mouse brain imaging–a simulation study," Phys. Med. Biol. **50**, 4609–4624 (2005).
[126]G. Bal, P. D. Acton, F. Jansen, and B. H. Hasegawa, "Revolving multipinhole SPECT for small animal imaging," IEEE Nucl. Sci. Conf. Rec. **1**, 5577–5584 (2008).
[127]P. L. Kench, J. Lin, M. C. Gregoire, and S. R. Meikle, "An investigation of inconsistent projections and artefacts in multi-pinhole SPECT with axially aligned pinholes," Phys. Med. Biol. **56**, 7487–7503 (2011).
[128]G. S. P. Mok, B. M. W. Tsui, and F. J. Beekman, "The effects of object activity distribution on multiplexing multi-pinhole SPECT," Phys. Med. Biol. **56**, 2635–2650 (2011).
[129]O. V. Makarova, G. Yang, P. T. Amstutz, and C. M. Tang, "Fabrication of antiscatter grids and collimators for x-ray and gamma-ray imaging by lithography and electroforming," Microsyst. Technol. **14**, 1613–1619 (2008).
[130]A. V. Ochoa, L. Ploux, R. Mastrippolito, Y. Charon, P. Lanièce, L. Pinot, and L. Valentin, "An original emission tomograph for *in vivo* brain imaging of small animals," IEEE Trans. Nucl. Sci. **44**, 1533–1537 (1997).
[131]B. W. Miller, J. W. Moore, H. H. Barrett, T. Fryé, S. Adler, J. Sery, and L. R. Furenlid, "3D printing in x-ray and gamma-ray imaging: A novel method for fabricating high-density imaging apertures," Nucl. Instrum. Methods Phys. Res., Sect. A **659**, 262–268 (2011).

[132]K. Deprez, S. Vandenberghe, K. Van Audenhaege, J. Van Vaerenbergh, and R. Van Holen, "Rapid additive manufacturing of MR compatible multi-pinhole collimators with selective laser melting of tungsten powder," Med. Phys. **40**, 012501 (11pp.) (2013).
[133]K. Deprez, "Preclinical SPECT imaging based on compact collimators and high resolution scintillation detectors," Ph.D. thesis, University Ghent, 2014.
[134]S. D. Metzler, R. Accorsi, J. R. Novak, A. S. Ayan, and R. J. Jaszczak, "On-axis sensitivity and resolution of a slit-slat collimator," J. Nucl. Med. **47**, 1884–1890 (2006).
[135]A. Sabbir Ahmed, G. H. Kramer, W. Semmler, and J. Peter, "Performance study of a fan-beam collimator designed for a multi-modality small animal imaging device," Nucl. Instrum. Methods Phys. Res., Sect. A **629**, 368–376 (2011).
[136]G. Muehllehner, "Effect of resolution improvement on required count density in ECT imaging: A computer simulation," Phys. Med. Biol. **30**, 163–173 (1985).
[137]F. H. Fahey, B. A. Harkness, J. W. Keyes, M. T. Madsen, and V. Zito, "Sensitivity, resolution and image quality with a multi-head SPECT camera," J. Nucl. Med. **33**, 1859–1863 (1992).
[138]M. T. Madsen, W. Chang, and R. D. Hichwa, "Spatial resolution and count density requirements in brain SPECT imaging," Phys. Med. Biol **37**, 1625–1636 (1992).
[139]Y. H. Lau, B. F. Hutton, and F. J. Beekman, "Choice of collimator for cardiac SPET when resolution compensation is included in iterative reconstruction," Eur. J. Nucl. Med. **28**, 39–47 (2001).
[140]C. Kamphuis, F. Beekman, and B. Hutton, "Optimal collimator hole dimensions for half cone-beam brain SPECT," in *Proceedings, Fully Three-Dimensional Image Reconstruction in Radiology and Nuclear Medicine* (Springer, Egmond aan Zee, The Netherlands, 1999), pp. 271–275.
[141]S. J. McQuaid, S. Southekal, M. F. Kijewski, and S. C. Moore, "Joint optimization of collimator and reconstruction parameters in SPECT imaging for lesion quantification," Phys. Med. Biol. **56**, 6983–7000 (2011).
[142]L. Zhou and G. Gindi, "Collimator optimization in SPECT based on a joint detection and localization task," Phys. Med. Biol. **54**, 4423–4437 (2009).
[143]M. F. Smith, S. Majewski, and A. G. Weisenberger, "Optimizing pinhole and parallel hole collimation for scintimammography with compact pixellated detectors," IEEE Trans. Nucl. Sci. **50**, 321–326 (2003).
[144]A. L. Weinmann, C. B. Hruska, and M. K. O'Connor, "Design of optimal collimation for dedicated molecular breast imaging systems," Med. Phys. **36**, 845–856 (2009).
[145]C. Robert, G. Montémont, V. Rebuffel, L. Verger, and I. Buvat, "Optimization of a parallel hole collimator/CdZnTe gamma-camera architecture for scintimammography," Med. Phys. **38**, 1806–1819 (2011).
[146]M. Rentmeester, F. van der Have, and F. Beekman, "Optimizing multi-pinhole SPECT geometries using an analytical model," Phys. Med. Biol. **52**, 2567–2581 (2007).
[147]S. T. Mahmood, K. Erlandsson, I. Cullum, and B. F. Hutton, "Design of a novel slit-slat collimator system for SPECT imaging of the human brain," Phys. Med. Biol. **54**, 3433–3449 (2009).
[148]S. Staelens, K. Vunckx, J. Debeenhouwer, F. Beekman, Y. Dasseler, J. Nuyts, and I. Lemahieu, "GATE simulations for optimization of pinhole imaging," Nucl. Instrum. Methods Phys. Res., Sect. A **569**, 359–363 (2006).
[149]B. M. W. Tsui, C. E. Metz, F. B. Atkins, S. J. Starr, and R. N. Beck, "A comparison of optimum detector spatial resolution in nuclear imaging based on statistical theory and observer performance," Phys. Med. Biol. **23**, 654–676 (1978).
[150]B. M. W. Tsui, "Letter," Phys. Med. Biol. **23**, 1203 (1978).
[151]R. F. Wagner and D. G. Brown, "Unified SNR analysis of medical imaging systems," Phys. Med. Biol. **30**, 489–518 (1985).
[152]R. F. Wagner, "Decision theory and the detail signal-to-noise ratio of Otto Schade," Photogr. Sci. Eng. **22**, 41–46 (1978).
[153]P. Sharp, D. C. Barber, D. G. Brown, A. E. Burgess, C. E. Metz, K. J. Myers, C. J. Taylor, and R. F. Wagner, "Medical imaging - The assessment of image quality," *International Commission on Radiation Units and Measurement, Bethesda, MD, ICRU Report 54*, *1996*.
[154]J. G. Ott, F. Becce, P. Monnin, S. Schmidt, F. O. Bochud, and F. R. Verdun, "Update on the non-prewhitening model observer in computed tomography for the assessment of the adaptive statistical and model-based iterative reconstruction algorithms," Phys. Med. Biol. **59**, 4047–4064 (2014).
[155]R. D. Fiete, H. H. Barrett, W. E. Smith, and K. J. Myers, "Hotelling trace criterion and its correlation with human-observer performance," J. Opt. Soc. Am. A **4**, 945–953 (1987).
[156]H. H. Barrett, J. Yao, J. P. Rolland, and K. J. Myers, "Model observers for assessment of image quality," Proc. Natl. Acad. Sci. U. S. A. **90**, 9758–9765 (1993).
[157]J. P. Rolland and H. H. Barrett, "Effect of random background inhomogeneity on observer detection performance," J. Opt. Soc. Am. A **9**, 649–658 (1992).
[158]M. P. Eckstein, C. K. Abbey, F. O. Bochud, J. L. Bartroff, and J. S. Whiting, "Effect of image compression in model and human performance," Proc. SPIE **3663**, 243–252 (1999).
[159]C. K. Abbey and H. H. Barrett, "Linear iterative reconstruction algorithms: Study of observer performance," in *Proceedings of the 14th International Conference on Information Processing in Medical Imaging* (Institute of Physics, London, Edinburgh, 1995), pp. 65–76.
[160]C. K. Abbey and H. H. Barrett, "Human- and model-observer performance in ramp-spectrum noise: Effects of regularization and object variability," J. Opt. Soc. Am. A **18**, 473–488 (2001).
[161]H. H. Barrett and K. J. Myers, *Foundations of Image Science* (Wiley-VCH, Weinheim, 2003).
[162]N. Fuin, S. Pedemonte, S. Arridge, S. Ourselin, and B. F. Hutton, "Efficient determination of the uncertainty for the optimization of SPECT system design: A subsampled fisher information matrix," IEEE Trans. Med. Imaging **33**, 618–635 (2014).
[163]L. Pato, S. Vandenberghe, B. Vandeghinste, and R. Van Holen, "Evaluation of Fisher Information Matrix approximation-based methods for fast assessment of image quality in pinhole SPECT," IEEE Trans. Med. Imaging (published online).
[164]L. Zhou, S. Kulkarni, B. Liu, and G. Gindi, "Strategies to jointly optimize SPECT collimator and reconstruction parameters for a detection task," in *IEEE International Symposium on Biomedical Imaging* (IEEE, Boston, MA, 2009), pp. 394–397.
[165]G. Zeng and G. Gullberg, "A channelized-hotelling-trace collimator design method based on reconstruction rather than projections," IEEE Trans. Nucl. Sci. **49**, 2155–2158 (2002).
[166]M. Defrise, A. Rezaei, and J. Nuyts, "Time-of-flight PET data determine the attenuation sinogram up to a constant," Phys. Med. Biol. **57**, 885–899 (2012).
[167]C. Vanhove, A. Andreyev, M. Defrise, J. Nuyts, and A. Bossuyt, "Resolution recovery in pinhole SPECT based on multi-ray projections: A phantom study," Eur. J. Nucl. Med. Mol. Imaging **34**, 170–180 (2007).
[168]L. Meng and N. Clinthorne, "A modified uniform Cramer-Rao bound for multiple pinhole aperture design," IEEE Trans. Med. Imaging **23**, 896–902 (2004).
[169]K. Vunckx, D. Bequé, M. Defrise, and J. Nuyts, "Single and multipinhole collimator design evaluation method for small animal SPECT," IEEE Trans. Med. Imaging **27**, 36–46 (2008).
[170]M.-W. Lee, W.-T. Lin, and Y.-C. Chen, "Design optimization of multi-pinhole micro-SPECT configurations by signal detection tasks and system performance evaluations for mouse cardiac imaging," Phys. Med. Biol. **60**, 473–499 (2015).
[171]E. Clarkson, M. A. Kupinski, H. H. Barrett, and L. Furenlid, "A task-based approach to adaptive and multimodality imaging: Computation techniques are proposed for figures-of-merit to establish feasibility and optimize use of multiple imaging systems for disease diagnosis and treatment-monitoring," Proc. IEEE Inst. Electr. Electron. Eng. **96**, 500–511 (2008).
[172]H. H. Barrett, L. R. Furenlid, M. Freed, J. Y. Hesterman, M. A. Kupinski, E. Clarkson, and M. K. Whitaker, "Adaptive SPECT," IEEE Trans. Med. Imaging **27**, 775–788 (2008).
[173]M. Freed, M. A. Kupinski, L. R. Furenlid, D. W. Wilson, and H. H. Barrett, "A prototype instrument for single pinhole small animal adaptive SPECT imaging," Med. Phys. **35**, 1912–1925 (2008).
[174]R. Van Holen, J. W. Moore, E. W. Clarkson, L. R. Furenlid, and H. H. Barrett, "Design and validation of an adaptive SPECT system: AdaptiSPECT," IEEE Nucl. Sci. Symp. Conf. Rec. **1**, 2539–2544 (2010).
[175]C. Chaix, J. W. Moore, R. Van Holen, H. H. Barrett, and L. R. Furenlid, "The AdaptiSPECT imaging aperture," IEEE Nucl. Sci. Symp. Conf. Rec. **1**, 3564–3567 (2012).
[176]M. Rozler and W. Chang, "Collimator interchange system for adaptive cardiac imaging in C-SPECT," IEEE Trans. Nucl. Sci. **58**, 2226–2233 (2011).